3.7 Plant Control

3.7.1 Introduction

A highly integrated plant control scheme is necessary for the efficient operation of the ITER device. This section describes the Plant Control System (3.7.2), which is composed of a number of subsystems: Supervisory Control System (3.7.2.2), Subsystem Control System (3.7.2.3), Interlock System and Fusion Power Shutdown System (3.7.2.4). Also described is Plant Operation Sequence (3.7.3), where various states of plant operation are defined and discussed. Finally, in section 3.7.4 magnetic, kinetic and disruption control are discussed.

3.7.2 Plant Control System

The ITER command control and data acquisition and communication (CODAC) system is structured in a hierarchy composed of the supervisory control system (SCS) and individual dedicated control subsystems to ensure the integrated control of the whole ITER plant. The CODAC system, through its supervisory system provides high level command to subsystems dedicated to the control and operation of each subsystem.

In the hierarchical structure of CODAC:

- subsystem controllers are supervised from the SCS;
- individual plant subsystems and diagnostic subsystems are directly controlled and monitored by their dedicated control systems;
- the limits in the autonomous behaviour of a subsystem are always determined by the SCS, allowing the possibility of going from complete autonomy during tests for example, to a total subordination when all parameters of the subsystem process are fixed from the supervisory control system.

To achieve integrated hierarchical control of the ITER plant, CODAC will provide general software functions for the benefit of the individual subsystems, a synchronization system, large bandwidth backbone communication networks with gateways and communication protocols which allow real time participation from remote ITER work sites. In addition, CODAC coordinates data acquisition & processing of data from the plant subsystems and manages the experimental database.

Software applications, common to many subsystems, will be provided by the SCS in order to make the control system as uniform as possible and to minimize the cost for design and maintenance. A formalism can be used to describe the logic of all operation sequences in a sequential function chart (SFC). For effective implementation, the same SFC methodology will be used for control and command design at all levels (supervisory or subordinate), for machine process operation and diagnostic data acquisition.

The individual subsystem SFC describes the logic of the subsystem control, operation, alarm and interlock functions. The subsystem also provides the instrumentation and control to implement the SFC logic. Data acquisition for plant subsystems will use conventional methods such as data scanning, data conversion, alarm limit checks and trend data processing.

With regard to the process of diagnostic data acquisition, the ITER tokamak operation will involve very long time scales, but events of interest will occur on short time scales. The length of the cycle for a given parameter would be controlled at a higher level so as to correlate with other timing signals. The memory would act as a buffer in line with the sensors.

3.7.2.1 Overall Plant Control System Function and Architecture

The ITER plant operation is controlled and monitored by the command control and data acquisition and communication (CODAC) system during normal operation modes. The CODAC system consists of a centrally positioned supervisory control system (SCS) and subcontrol systems dedicated to each plant subsystem under the supervision of the SCS. A concept of ITER control system is schematically shown in Figure 3.7.2-1.

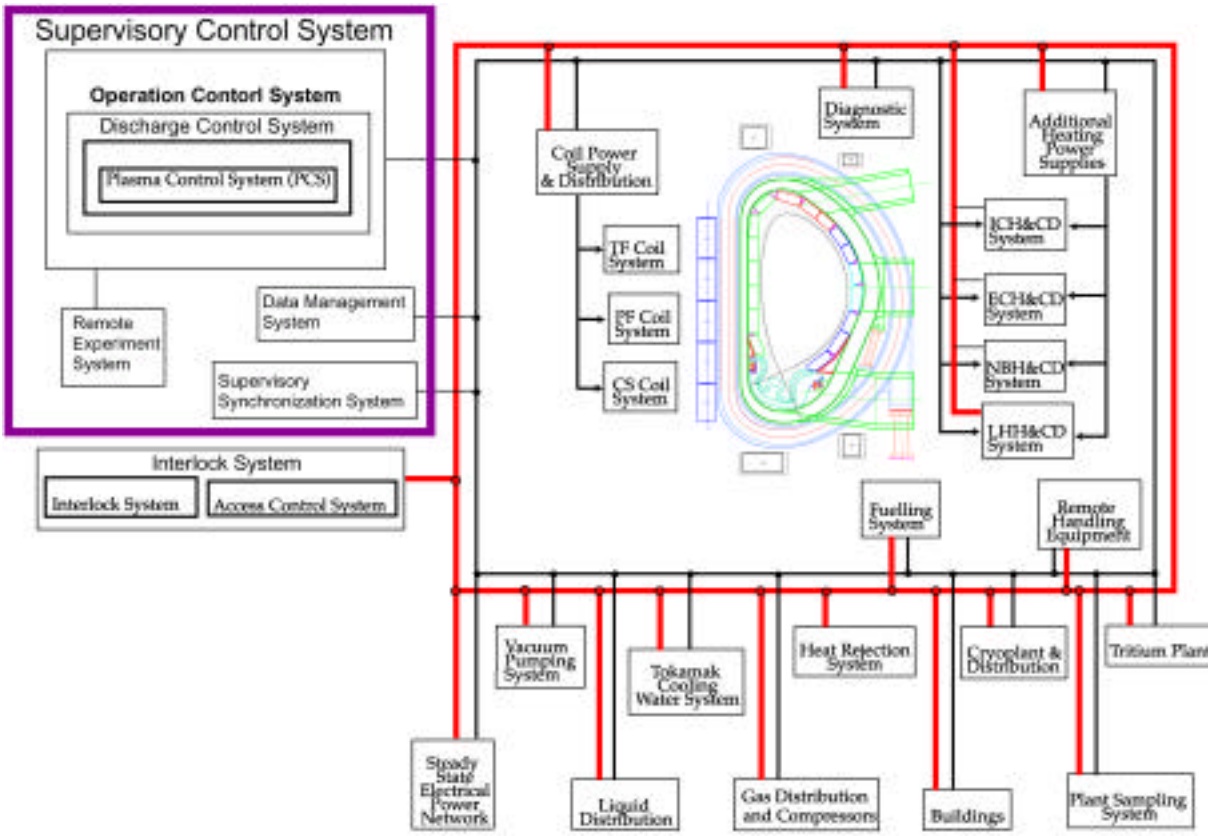

Figure 3.7.2-1 ITER Control System

The SCS controls transition of the entire ITER plant operation state, and provides high level commands to plant subsystems, in order to achieve integrated control of the entire plant. The SCS also monitors the operation state of each plant subsystems to ensure it is operating within the proper operational envelope of the ITER plant operation state.

The interlock system, in parallel with the CODAC system, ensures plant-wide machine protection, as well as personnel protection, in case of off-normal events. In addition, the interlock system monitors operational events of the plant, and performs preventative and protective actions to maintain the system components in a safe operating condition. The

interlock system is also hierarchically structured and has individual interlock subsystems which are dedicated to each plant subsystem.

The fusion power shutdown system (FPSS) is the safety class plasma shutdown system used in case of an off-normal events. The FPSS is triggered by detection of off-normal events occurring in the tokamak cooling water system (TCWS).

3.7.2.2 Supervisory Control System

3.7.2.2.1 Functions

The SCS supervises the ITER plant operation, controls the plasma discharge, imposes selected plasma parameters, acquires plant and scientific diagnostic data, displays alarms, creates the ITER database, and communicates with both on-site and remote site control rooms. The functions of the SCS are summarized as follows:

- Overall ITER plant operation, management and data monitoring;
- Plasma discharge sequence management;
- Plasma operation support;
- Diagnostic data processing support;
- Data management of experimental results;
- The synchronisation system for plasma discharge and data acquisition;
- Communication functions and communication networks;
- Remote-site experiment capability;
- Plasma control system (PCS).

3.7.2.2.2 System Architecture

Operation control system
This provides the supervisory function of the ITER operation state management, and configuration control at the highest level of the control architecture. When the ITER plant is in a plasma operation state, operation of the plant and the discharge sequence are managed and controlled by the discharge control subsystem (DCS). When the ITER plant is ready to initiate plasma operation, the PCS will assume responsibility for controlling the ITER device components and systems which directly affect plasma operation. After completion of the plasma discharge operation and resetting of the system, the control is returned back to the DCS. The PCS has four major functions: plasma operation scenario sequencing, plasma magnetics control, plasma kinetics and divertor control, and fast plasma shutdown. It also displays monitoring signals for the plant operation. Relations between the phases controlled by DCS and PCS are shown in Figure 3.7.2-2. Throughout these operation sequences and phases, the operation control system always maintains the ultimate responsibility for operation, control and protection of the ITER facility and device.

Machine data acquisition system :
This also globally monitors all plant subsystems and interlocks.

Diagnostic control and data acquisition system:
This provides the supervisory function of the ITER diagnostic subsystem control and operation, configuration control and plasma parameter computation.

Data management system :
This provides the supervisory function of the creation and management of the ITER experimental database as well as data storage and archiving. In addition, it also provides a computational capability for detailed data analysis.

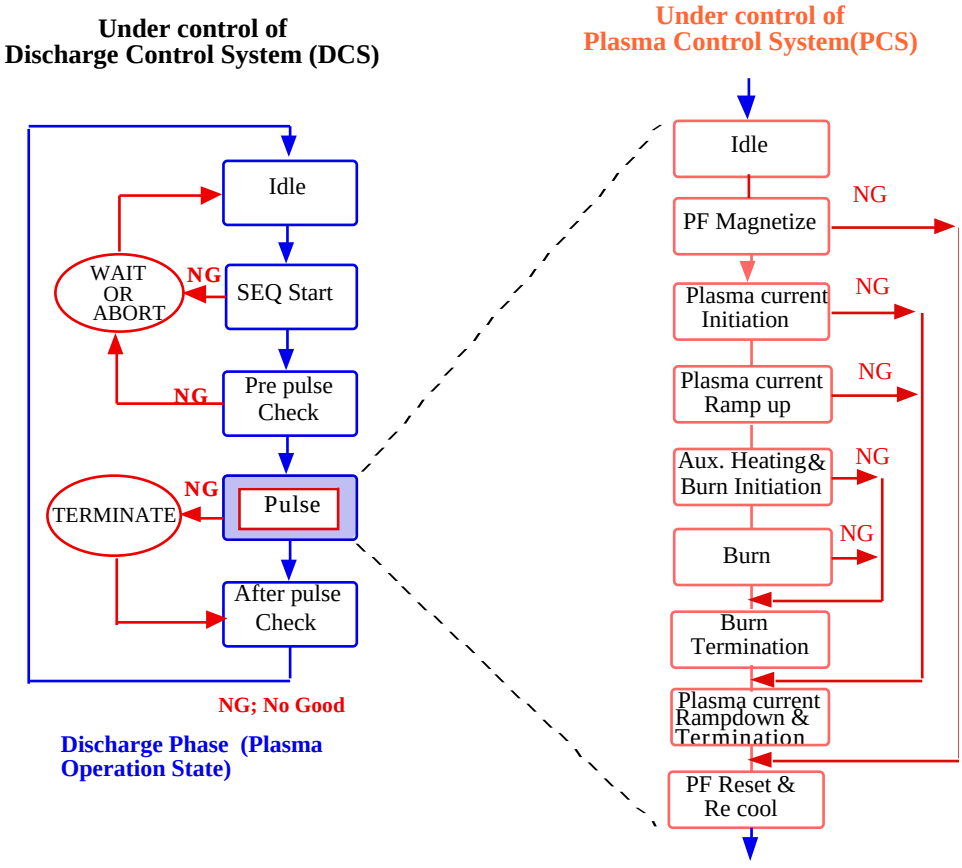

Figure 3.7.2-2 Plasma Discharge Control Phase

Supervisory synchronisation system :
This provides the supervisory function of the synchronisation system which consists of the master clocks, clock distributions, timing signal input/output portions and their logic control.

Supervisory network and communication system :
This provides the supervisory backbone networks and message communication software, which handle all data and command communications among the entire ITER plant control system. This communication software will be used for all ITER subsystems as a standard software package.

Remote experiment system :
This provides the wide area network (WAN) node processor to communicate with each remote work site. The necessary information from the ITER plant and experimental database

are extracted through each subsystem of SCS, which also communicates with individual subsystems if required through the ITER CODAC network and WAN node processor.

Plasma Control System (PCS):
The scope of plasma control and the corresponding requirements for the PCS comprises four major categories:

- Plasma operation scenario sequencing: (see 3.7.3.2)
- Magnetics control: (see 3.7.4.1)
- Kinetic control: (see 3.7.4.2)
- Disruption Control: (see 3.7.4.3)

3.7.2.3 Subsystem Controllers

The CODAC system is structured in a hierarchy composed of the SCS and individual dedicated control subsystems to ensure integrated control of the entire ITER plant. The Control subsystems need to satisfy the following requirements:

- subsystem controllers are supervised by the SCS;
- individual plant subsystems and diagnostic subsystems are directly controlled and monitored by their dedicated control subsystems;
- limits in the autonomous behaviour of a subsystem are always determined by the SCS, allowing for the possibility of going from complete autonomy during tests to a total subordination when all parameters of the subsystem process are fixed by the SCS.

The ITER plant control system is composed of the following subsystem controllers (with the exclusion of diagnostics):

1) TF, CS, PF coils, correction coils and structure instrumentation and control system (includes power supply control for coil system);
2) Vacuum vessel (VV), blanket, divertor instrumentation system;
3) Pellet fuelling instrumentation and control system;
4) Gas fuelling instrumentation and control system;
5) Wall conditioning instrumentation and control system;
6) Tokamak cooling water and CVCS control system;
7) Vacuum pumping control system (includes cryostat instrumentation);
8) Tritium plant control system;
9) Cryoplant control system (includes cryostat instrumentation);
10) RF power supply and control system (IC, EC and possibly LH);
11) NB power supply and NB control system;
12) Steady state power supply control system;
13) Radiation monitoring system;
14) Liquid and gas distribution control system;

The individual control subsystems have similar functions to the SCS, but perform their dedicated duties for operation, control and data acquisition. These are:

- Control of operations:
- Alarm handling:
- Monitoring and display:
- Data acquisition and storage:
- Synchronisation:
- Data communication:

3.7.2.4 Interlock System and FPSS

The interlock system, through its supervisory system, ensures plant-wide machine protection as well as personnel protection with graded approach, and must act rapidly and directly in case of off-normal events or conditions. For that reason, the interlock system is fully independent of the CODAC system except for the data monitoring communication bus, which is shared with CODAC.

The FPSS secures the safe shutdown of the fusion power in case of an ex-vessel coolant leakage. Off-normal events will be displayed and recorded. A dedicated network will be used for off-normal event detection and dispatch of the command signal to the fuelling system for power shutdown. Because of its dedicated safety function, the FPSS is independent from other interlock systems.

3.7.2.5 Functional Interface between CODAC, Interlock System and FPSS

Reliable operation of the ITER plant will be achieved through an integrated plant control. The CODAC has the primary function of maintaining the plant operating condition in normal states. The interlock system tries to avoid or minimise machine damage from operational events with or without availability of the CODAC. This is why the interlock system is separated from the CODAC and FPSS.

Even though the interlock system is in principle designed to be independent of the CODAC, some level of coordination between the interlock and CODAC systems will be essential. Some interlock actions can be executed by the CODAC as long as it is operational. Also, the interlock system is a back-up machine protection system in case of CODAC failure.

In general, the interlock protective actions are graded at three levels:

Level 1: (fast shutdown)
Whether the CODAC is functional or not, plasma discharge is terminated by the direct command of the interlock system. Possible scenarios are as follows:
- immediate shutdown by D_2 gas injection;
- immediate shutdown by the killer pellet injection ;
- immediate shutdown of auxiliary systems like additional heating systems.

Level 2: (fast or accelerated shutdown)
Detected deviation of the process value from the normal operation range is not as gross as the case of Level 1. Compared with the Level 1 interlock actions, slower actions are expected.

Interlock actions will be executed through the coordinated operation of the CODAC. The following scenarios are presently foreseen:

- A time delay (~ 150 s) will be set after the interlock trigger expecting a recovery by the normal control function of the CODAC during this delay period. After a certain delay time (~ 150 s), if the recovery is not yet achieved, a fast shutdown will be triggered.
- The interlock system requests the SCS to shift the discharge phase to fast or accelerated plasma shutdown phase (~ 150 s).

Level 3: (shot sequence inhibition)

Compared to the previous two levels of interlock events, this is a case of minor deviation of the interlock process values, which does not require immediate termination of the discharge.

- The discharge sequence will be stopped if it is prior to the plasma initiation;
- If the plasma is already initiated, the plasma discharge will be completed but the following discharge sequence will be suspended;
- In case of discharge cleaning such as EC discharge cleaning, this interlock event stops the sequence immediately.

Set point on certain process value for interlock event trigger will be shown in Figure 3.7.2-3 for illustrative purposes.

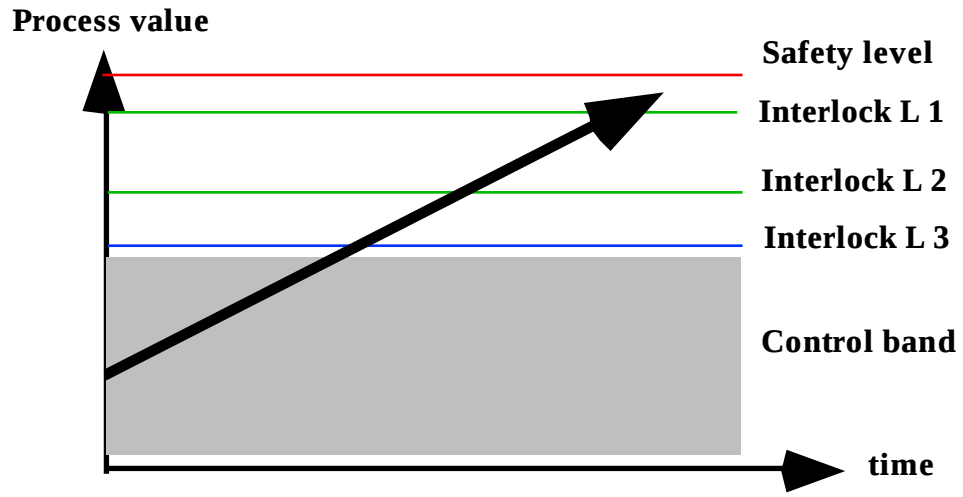

Figure 3.7.2-3 Interlock Level Set Point

When a process value deviates beyond its interlock Level 1 set point value and reaches the safety system trigger level, the safety system is then activated for reliable and robust shutdown of the system. FPSS is one of the safety systems which shuts down the fusion power production in case of an off-normal event such as ex-vessel coolant leakage. In this case the FPSS monitors the primary heat transfer system coolant parameters for the safety event trigger.

Functional relations between CODAC, interlock and FPSS are summarised in Figure 3.7.2-4.

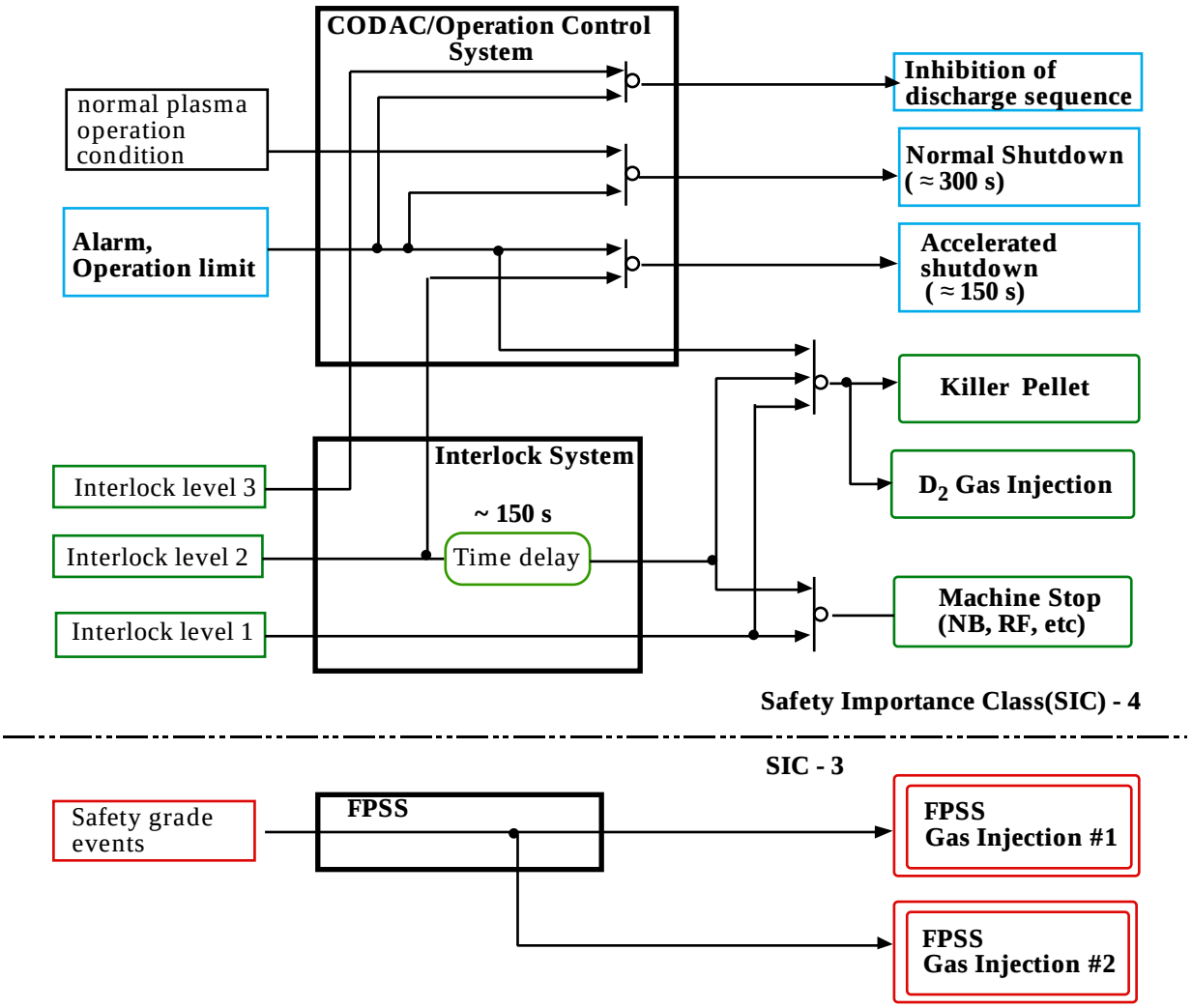

Figure 3.7.2-4 Functional Relations between CODAC, Interlock, and FPSS

3.7.3 Plant Operation

This section schematically describes the operational sequences of the ITER plant by using a sequence function chart (SFC). A SFC describes the control process for the plant using an implementation-independent graphical representation.

The process described by the SFC can be divided into a number of well-defined, successive "steps", separated by "transitions". The purpose of each step, when it becomes "active", is to launch new actions. The subsequent transition of the system describes a condition or conditions that must occur before the next step can become active. The "state" of part of the plant may indicate the last step it passed (e.g. "operating"), or in which transition it is engaged (e.g. "waiting for temperature to reach 200˚C").

Macroscopically, the operation of the ITER plant is characterised by major plant states, in which most of the plants are waiting for some command before relatively rapidly changing to another state, and some plant items are undergoing maintenance or testing, or are in operation.

Construction and Long-Term Maintenance State (LTM)
This state is applied to periods of major machine modification. Long term maintenance is defined as that taking >30 days. In this state, most of the tokamak subsystems which require maintenance may be shut down. Decay heat is passively removed. For example, the cryoplant may be shut down, the VV and cryostat may not be actively pumped, and large in-vessel and ex-vessel component replacement and maintenance may be conducted. Coil excitation and any power injection by an additional heating system to the tokamak is prohibited.

Short-Term Maintenance State (STM)
This state allows maintenance activities which typically last for 1 to 30 days. Relatively long time periods of plasma operation stoppage such as night times and weekends may require that the plant be placed in this state with reduced or without toroidal field coil current. Decay heat removal may be taking place, if appropriate. In this state, component maintenance and replacement needs to be carried out under high vacuum conditions in the VV and, if in the cryostat, also under cryogenic temperature conditions. The vacuum and cryogenic temperature conditions must also reach or regain their operational levels during this state. PF coil excitation is prohibited in this state.

Test and Conditioning State (TCS)
Wall conditioning operations such as baking, glow discharge cleaning and EC discharge cleaning, with or without baking, are major actions. TF and PF coil excitation tests may be carried out. Additional heating system tests such as NBI ion source conditioning, RF dummy load tests, and fuelling system tests are allowed without any tokamak plasma. During the TCS no in-vessel or major ex-vessel maintenance may be initiated. However, minor ex-vessel component maintenance and trouble-shooting is allowed outside the pit area.

Short-Term Standby State (STS)
Final preparation of each subsystem is completed and all systems are ready for plasma operation. Limited troubleshooting is allowed within 8 hours of the last pulse. Maintenance and conditioning operations are not allowed.

Plasma Operation State (POS)
All of the plant subsystems are supervised or directly receive commands from the SCS during plasma operation. No maintenance activities are allowed in this operation state.

3.7.3.1 Overall Plant Operational Sequences

The relationship between states can be presented by the sequential function chart, shown in Figure 3.7.3-1. The basic direction of evolution in the chart is from top to bottom unless indicated by arrows. Operation sequences covering the transfers between states are macroscopically represented by boxes labeled SEQn (n=1–10).

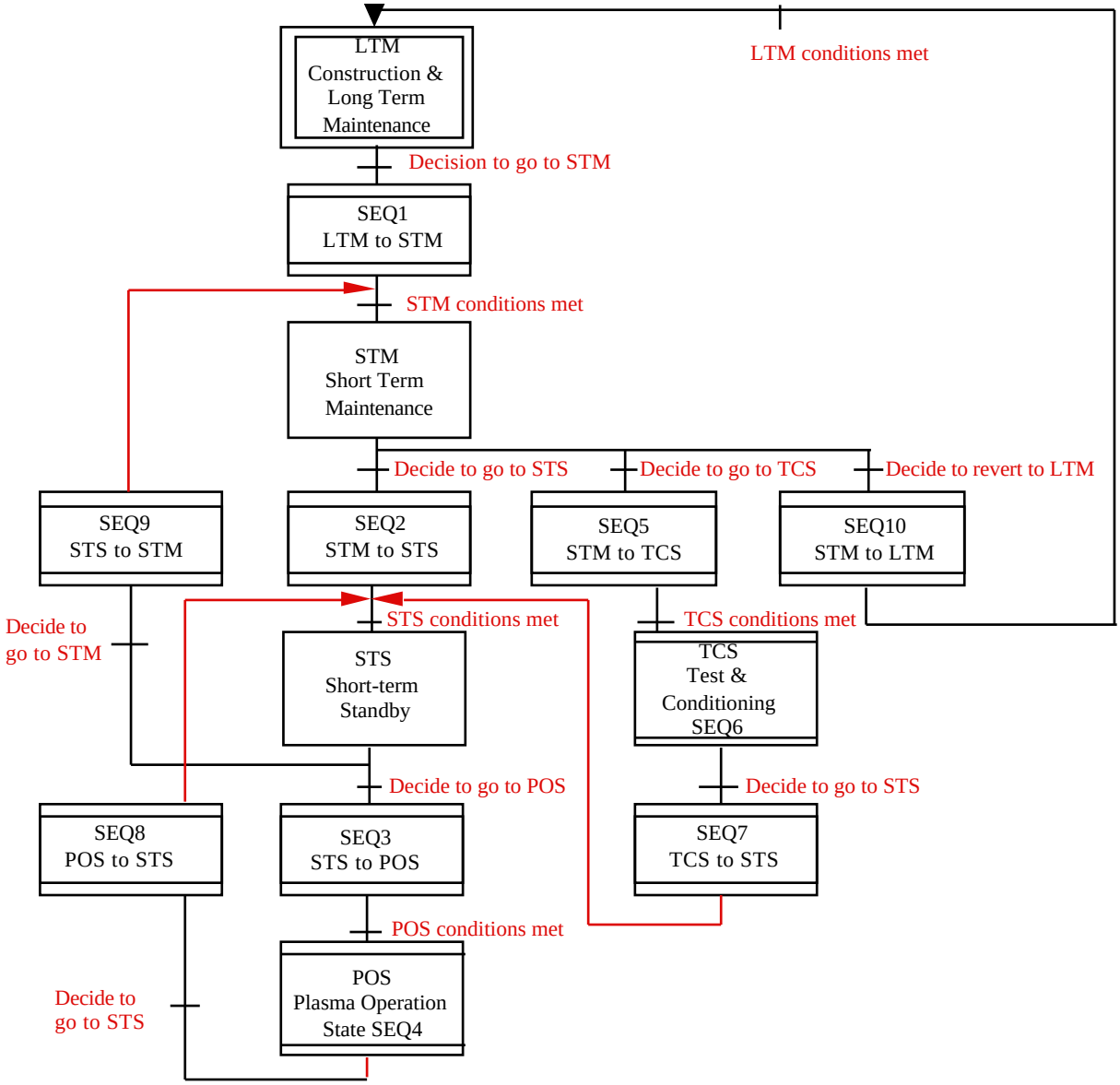

Figure 3.7.3-1 ITER Plant State Transitions

3.7.3.2 Plasma Operation Sequences

When ITER is permitted to operate and produce plasma pulses, operation of the plant is managed and controlled by the discharge control subsystem (DCS). When the ITER plant is ready to initiate the plasma pulse, the plasma control system (PCS) will assume responsibility for controlling ITER device components and systems which directly affect plasma operation. DCS and PCS mainly play the role of supervisory control and each subsystem under DCS and PCS has its own dedicated local control system.

After completion of the plasma pulse and resetting of the system, control is passed back to the DCS. This operational sequence of the control system is shown in Figures 3.7.3-2 and 3.7.3-3.

First, the discharge parameters are selected and transferred to the DCS. After checks for consistency of these discharge parameters, the discharge sequence will be started. First, pre-pulse checks will be carried out for the availability and operational readiness of all the necessary plant systems. After these tests are completed and satisfied, the PCS will take over the control of tokamak-related operation.

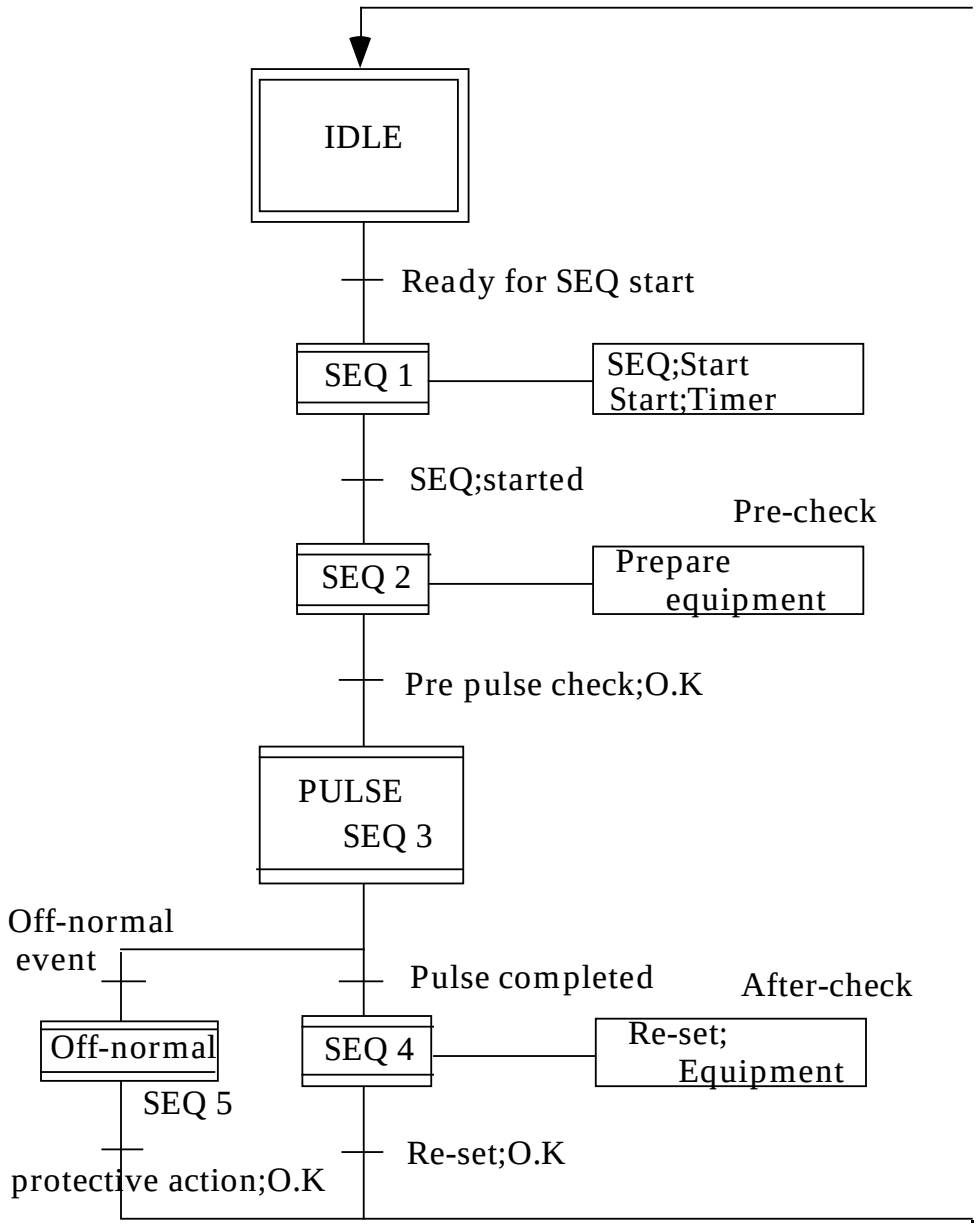

Figure 3.7.3-2 Overall Plasma Pulse Sequence

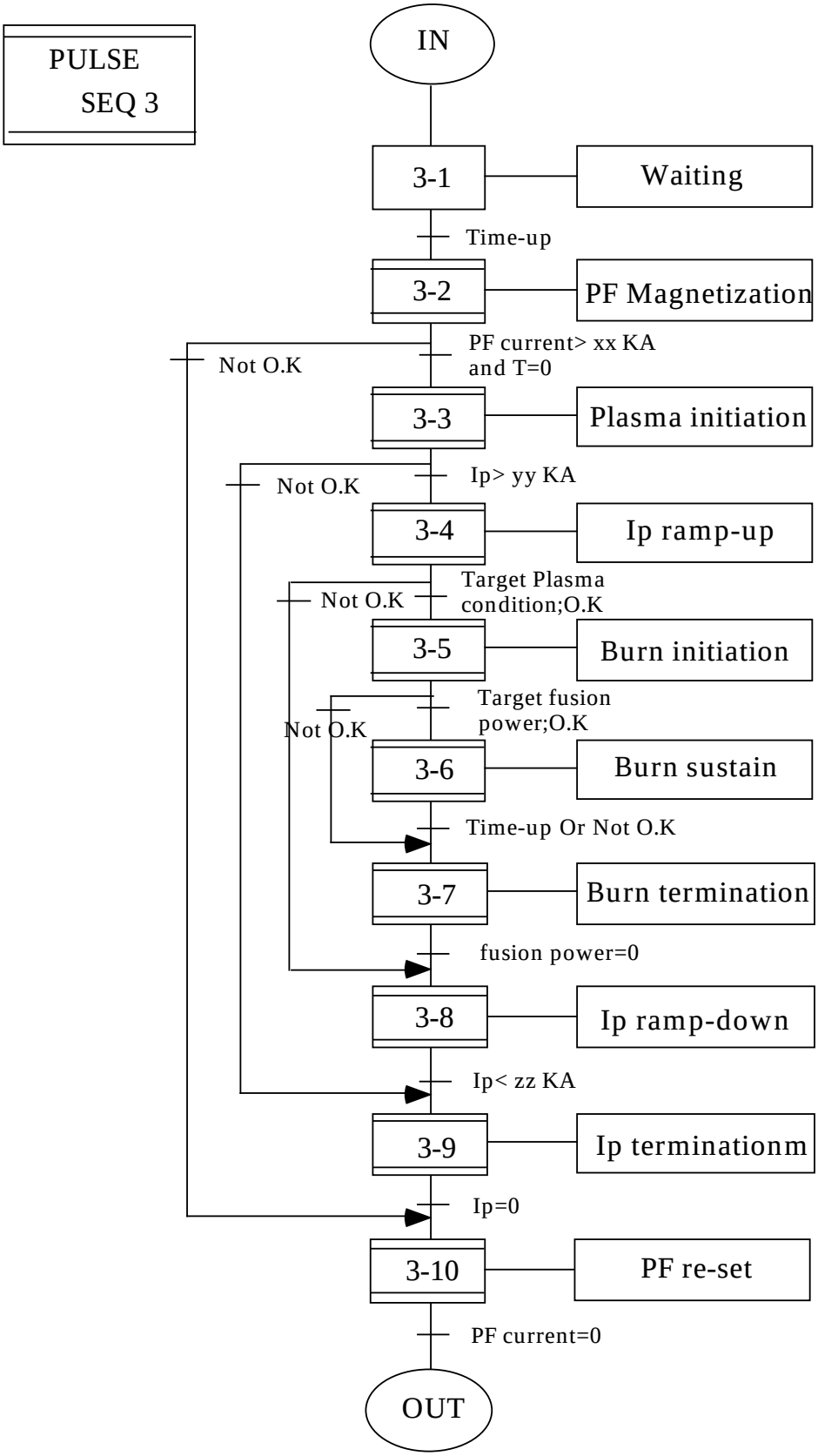

Figure 3.7.3-3 Detailed Sequence of "Pulse" State (SEQ.3)

Figure 3.7.3-4 illustrates the key features of plasma operation scenarios. The parameters of the scenario – current, fusion power, auxiliary heating and/or current drive input and burn duration – can vary, but the sequencing requirements and general waveforms remain invariant.

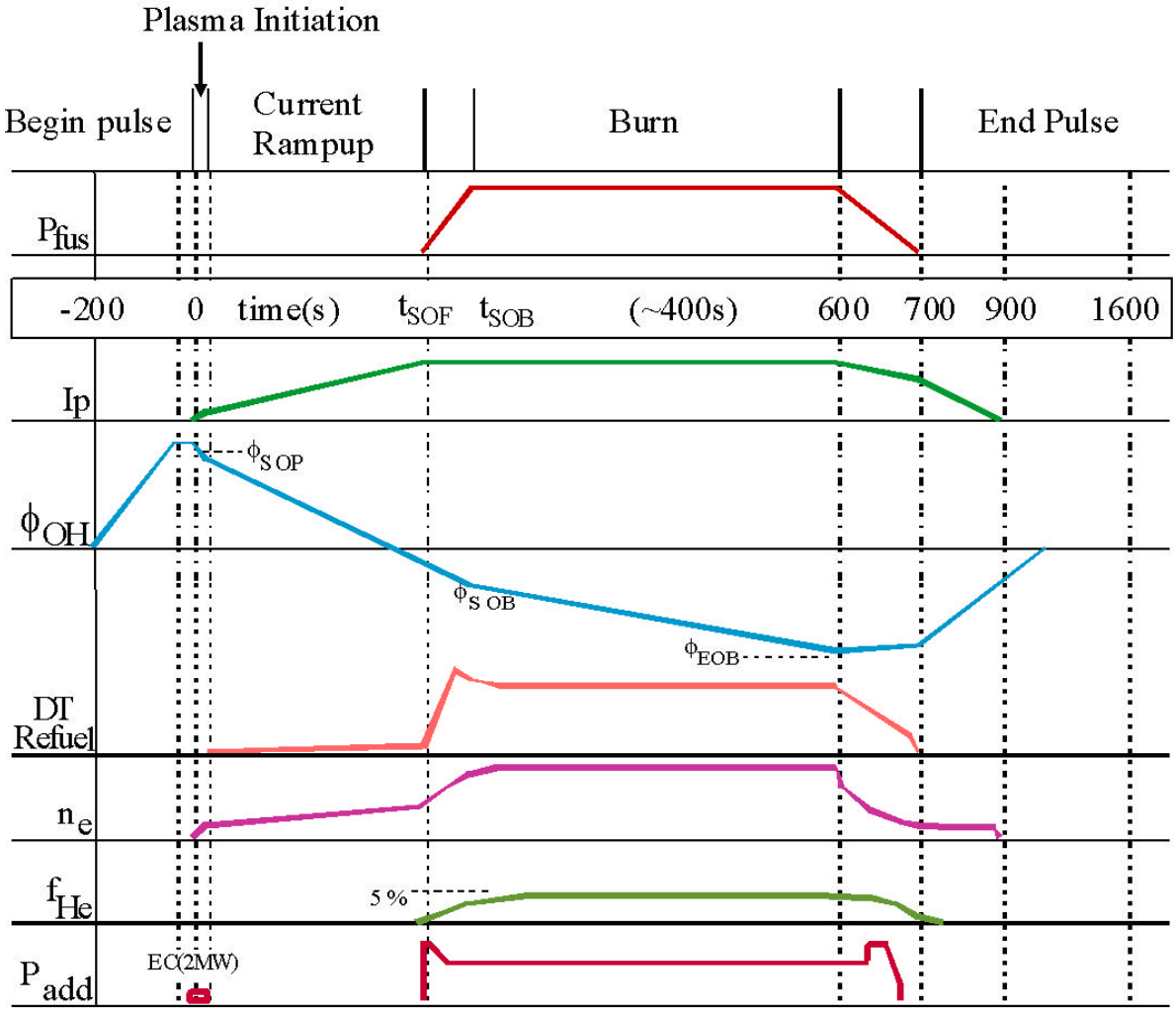

Figure 3.7.3-4 Waveforms for Standard Driven-burn Operation Scenario

3.7.3.2.1 Plasma Discharge Sequence

Plasma Initiation

A pulse proceeds from pulse initiation with attainment at t = 0 of PF coil system pre-magnetisation with a plasma-axis flux linkage of φ_{SOP}(start of pulse), as shown in Figure 3.7.3-4. This is followed by a 2 s plasma initiation phase that begins with the application of pre-determined voltages to the PF coils. These voltages and the initial PF currents are chosen to produce a dynamic multipole field null with a low poloidal field (< 2 mT within an 0.8 m radius) that is positioned near the port-mounted start-up limiters at t ≈ 1 s. The in-vessel loop voltage is ~ 12 V (E ≈ 0.3 Vm^{-1}) at this time. With a gas fill pressure of about 1.3 mPa, Townsend avalanche breakdown occurs within 50 ms.

During start-up, 2 MW of EC power at 120 GHz will be provided for 2 s to facilitate initial breakdown over a range of pre-fill pressures and error-field conditions, and will also provide supplemental heating after breakdown to ensure rapid ionisation (burn-through) of impurities in the initial low-current startup plasma.

Current Ramp-up

The current ramp-up with average dI/dt ≈ 0.15 MAs^{-1} is coordinated with a minor radius expansion and elongation increase to maintain a nearly constant edge safety factor $5 \leq q \leq 6$. The plasma remains limited until I_{SOD} (start of divertor) ($\approx 0.5\ I_{P0}$) is reached, when a single null (SN) divertor configuration is formed ($q_{95} \approx 4$). Continuation of the current ramp-up results in an I_{P0} current flat-top ($q_{95} \approx 3$) at $t \approx 100$ s.

Shape and Configuration Control

Dynamic control of the plasma shape and position is required throughout the scenario. The clearance gap between the first wall and the separatrix are controlled, in particular near the outboard equatorial plane to permit and efficient coupling to the plasma from IC and LH launchers.

Heating to Driven Burn

Following SOF (start-of-flat top), auxiliary heating is applied. This, coordinated with plasma fuelling, results in the attainment of H-mode confinement and sustained fusion burn with ~ 500 MW of fusion power within ~ 50 s. Attainment of the rated fusion power is denoted as the start-of-burn (SOB). The most demanding requirement in this phase is the transition from L to H mode confinement, which requires that a certain threshold heating power, linked with plasma density, be provided. It is assumed that the required plasma shape and current are achieved at SOF and that plasma heating and β increases are carried out at constant shape and current. Scenarios, which modify plasma shape and current during the plasma heating before SOB, can also be considered.

In extended-pulse-duration/steady-state operation, the scenario is more complicated. Following SOF, auxiliary power heats the plasma and generates a toroidal current which, together with the bootstrap current, replace the Ohmic current. Generally, the current profile before the addition of auxiliary power is somewhat different from the final profile. The current diffusion time across the whole plasma volume is large, e.g. ~ 200 s for $T_e \approx 5$ keV and ~ 800 s for $T_e \approx 10$ keV. So during the sustained burn, the current profile will evolve to the final state over several 100 s.

Sustained Burn

Once SOB is attained, accumulation of thermal helium results in the need to further increase the plasma density to maintain a fixed fusion power: the approach to sustained burn with stationary helium level requires a few tens of seconds. The burn proceeds until the end-of-

burn (EOB) inductive flux limit of the PF coil system is reached. For nominal conditions, the duration from SOB to EOB is about 400 s for the driven-burn.

Burn Termination

The burn is terminated by reducing the fuelling to ramp-down the fusion power, followed by current, auxiliary heating and density ramp-down and plasma termination, with measures to avoid plasma disruptions.

3.7.3.3 Off-normal Plant Operation Sequences

ITER plant off-normal conditions are classified following three different levels of protection from relation to the ITER plasma discharge:

Level 1; fast plasma termination
Level 2; controlled plasma termination
Level 3; pulse inhibition

All of the Off-normal events are classified into above three levels of protection and initiate corresponding actions when off-normal events are enabled at any operation state. Individual subsystem component protective actions such as coil fast discharge, slow discharge, additional heating power off, isolation from leakage are also included within above protections. Figure 3.7.3-5 represents the scheme of actions for off-normal event.

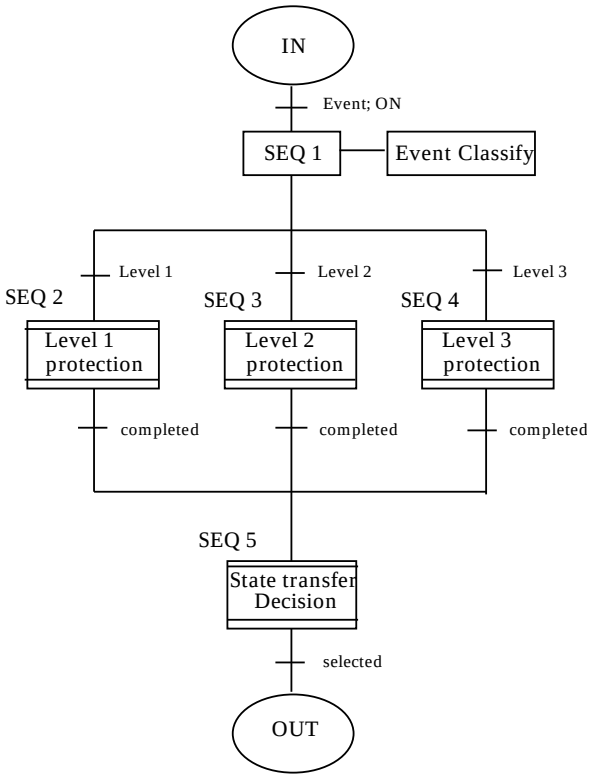

Figure 3.7.3-5 Overall Off-Normal Sequence

3.7.4 Magnetic and Plasma Control

Plasma control is an essential element to achieve the goals of the ITER experimental programme. Its objectives include machine protection and plasma operation. Successful plasma operation requires a control system monitoring the plasma status by diagnostic sensor signals and able to counteract the deviations from the reference values by controlling the relevant actuators. A list of sensors and actuators needed for plasma control is shown in Table 3.7.4-1.

Table 3.7.4-1 Sensors and Actuators for Plasma Control

Category	Sensor or Indication	Actuator or Action
Key machine protection	Gaps between the separatrix and first wall/divertor, first wall temperature	PF coils
	Fusion power	P_{add}, fuelling/pumping
	Div. Plate temperature	Impurity gas-puff in divertor
Additional machine protection (disruption)	Disruption precursors (particularly detection of locked modes)	I_p, P_{add}, fuelling/pumping, killer pellet
	Halo currents	
	Runaway electrons	PF coils ($q<2$)
ELM heat load	Type of ELM, divertor plate. temp.	I_p, shaping, fuelling/pumping, selection of PFC
Shine-through	Shine-through power, n_e	NB
Plasma-wall contact	Impurity emission lines	PF coils
Conventional control	B_p, flux loop	PF coils
	I_p	PF coils
	n_e	fuelling/pumping
Burning plasma control	Fusion power	P_{add}, fuelling/pumping
	Divertor heat load	Impurity seeding, fuelling/pumping
	Helium ash, impurity	Fuelling/pumping
Beta	Stored energy	P_{add}, fuelling/pumping
Threshold power	Fusion power, P_{rad}, n_e	P_{add}, fuelling/pumping
Advanced control	q profile	CD, P_{add}, fuelling/pumping
	Pressure profile	
	Rotation profile	
Neoclassical tearing mode control	NTM mode amplitude and location	ECCD, saddle coils
Resistive wall mode control	RWM mode amplitude, phase	Saddle coils

The first set of control loops, shown with bold letters are categorised as machine protective control. Machine protective control involves prediction, avoidance and mitigation of disruptions and avoidance of abnormal heat loads to protect the components inside the vacuum vessel. The control in this category has the highest priority and the control commands generated thereby override the other control commands.

Some control loops aim at protecting key machine components, these include the monitoring of the gaps between the separatrix and first wall/divertor, wall/divertor temperature and fusion power, the detection of contact of the plasma to the wall, of excessive heat to the divertor, and of unwanted excursions of fusion power. Wall contact of the plasma can be detected by impurity line emission or by magnetic signals. Such an event would invoke correction of plasma position and shape, increase of radiation power, and reduction of auxiliary heating and fuelling.

Other control loops are for additional machine protection against disruption. Protection of components inside the vacuum vessel requires failure-free detection of disruption precursors, avoidance, and mitigation of disruptions. The precursors of disruptions can be detected by monitoring the fluctuation of the magnetic signals and ECE and soft X-ray emission. Of particular importance is the recognition of locked modes. Recently, disruption detection systems have been developed using neural networks. Once a disruption is recognised in advance, it may be avoided by reducing the plasma current, β, or density. A decision has not yet been made on whether to include a killer pellet injection system to distribute the plasma energy over a large area to mitigate the consequences of disruption, on the understanding that adequate plasma termination can be achieved using an edge impurity gas puff. The runaway electrons can be eliminated by shifting the plasma and reducing the edge safety factor to 2.

Finally, some additional control loops are for ELM heat load control. This system recognises the type of ELM and measures the divertor heat load associated with it. If the heat load due to ELMs is excessive, the operation has to be shifted to a regime with more benign ELMs. Possible methods include increasing the fuelling rate, increasing the safety factor, and changing the plasma geometry.

The set of controlled plasma parameters will include those currently considered in the present generation of tokamak plasmas, in particular the plasma shape and position, the plasma current, and the electron density. Operation with a burning DT plasma results in additional plasma control requirements, in particular a simultaneous control of the fusion power, divertor heat load and helium-ash is needed. The ITER divertor is designed for a high steady state peak power load but, at full power, a substantial fraction (~ 75%) of the total power must be radiated to keep the power deposited on the divertor plates to acceptable levels. This operation may require injection of a controlled amount of a specific impurity or a combination of impurities (e.g. Ne, Ar) to the divertor and scrape-off layer (SOL) plasma but, at the same time, the bremsstrahlung power loss and plasma dilution in the core must be maintained at acceptable levels for the plasma burn. The kinetic control must also keep the plasma away from the β and density limits and provide sufficient power flow through the separatrix to ensure H-mode plasma operation. It is clear that a sophisticated multi-input, multi-actuator feedback control scheme is required for the successful operation of ITER even in the basic driven burn regime. Therefore a wide range of additional plasma measurements is required for control, including radiative power loss from the plasma core, SOL, X-point region and from the divertor, plasma density profile, β, n_T/n_D ratio, rotating MHD modes, and the degree of divertor detachment, i.e. “ionisation front” position and/or T_e and n_e at the divertor plate.

Further, sustained operation in high confinement modes, for example reverse shear, is a fundamental part of the ITER experimental programme. This operation is likely to require control, and hence measurement of the spatial profile, of key parameters such as q, pressure and rotation. For sustained operation near the β-limit, it is expected that detection and suppression of neoclassical tearing modes (NTMs) will be required, and for resistive wall modes (RWMs) in steady state operation at high β levels. Measurement of the location and amplitude of these modes, and active stabilisation by ECCD and saddle coils, will therefore be required.

3.7.4.1 Plasma Control by the Poloidal Field System

3.7.4.1.1 Requirements of the Poloidal Field System

The ITER poloidal field (PF) system has been designed to support all the design scenarios (the first four scenarios from Table 3.7.4-2). Its overall operational flexibility was also assessed by studying the feasibility of a high current scenario. This is named scenario 5 in the table below and reaches 17 MA of plasma current (fusion power 700 MW, Q = 20).

Table 3.7.4-2 Plasma Current (MA) at the Key States of the Scenarios

State	SOD	XPF	SOH	SOB	EOB	EOC
Scenario 1	0	7.5	13	15	15	12.3
Scenario 2	0	7.5	15	15	15	12.3
Scenario 3	0	7.5	9.5	13.5	13.5	11
Scenario 4	0	5.4	7	9	9	8
Scenario 5	0	7.5	15	17	17	13.2

For each scenario seven key states were identified: the start of the magnetised central solenoid (CS) discharge (SOD), the X-point formation (XPF), the start of plasma additional heating (SOH), the start of plasma current flat-top (SOF), the start of driven burn (SOB), the end of burn (EOB) and the end of plasma cooling (EOC). Table 3.7-2 shows the values of plasma current at these key states. Up to XPF the plasma touches the central part of the limiter. The PF system drives the plasma cross-section expansion during the current rise, keeping the edge safety factor roughly constant at a value of about 4.8. At XPF, transition from a limited to a fully developed diverted configuration takes place. Further ramp-up of the plasma current continues in the diverted configuration.

As an example, Figure 3.7.4-1a shows the evolution of the plasma aperture during the current ramp-up in scenarios 1 and 2. In scenario 2, additional heating is initiated at the start of the current flat-top. In all other scenarios, the SOH is before SOF. At EOB, a controlled termination of the fusion burn is initiated. The plasma must be cooled prior to the current ramp-down, in order to avoid the large negative currents at the plasma edge arising when a negative surface voltage is applied. Finally, at EOC, the transition from a diverted to a limited configuration takes place.

The plasma in scenarios 1, 2, 3 and 5 is characterised, during the current flat-top, by the following parameters: R = 6.2 m, a = 2 m, $\kappa_{95} \approx 1.70$, $\delta_{95} \approx 0.33$. The plasma of scenario 4 (at burn) is shifted outwards: R = 6.35 m, a = 1.85 m. This plasma has higher elongation, $\kappa_{95} \approx 1.85$, and higher triangularity, $\delta_{95} \approx 0.42$, than the standard plasma of scenarios 1, 2, 3 and 5. Table 3.7.4-3 presents the values of the plasma main parameters during the driven burn. Figure 3.7.4-1b shows the overlay of the separatrices of the inductive scenarios and of scenario 4 during the burn.

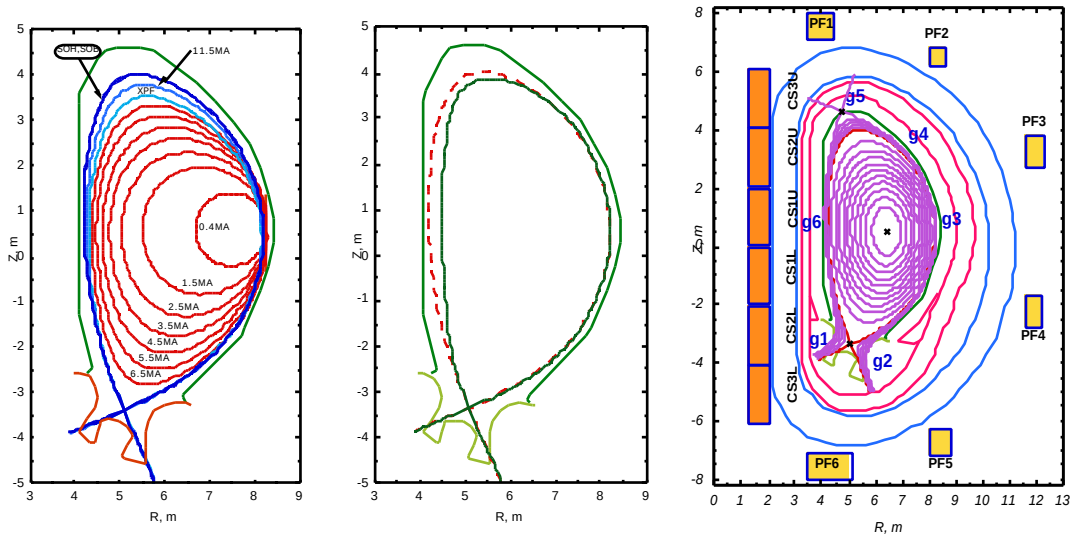

a **b** **c**

Figure 3.7.4-1a - Plasma Boundary during the Current Ramp-Up, Heating and Burn Phases of Scenarios 1 and 2; b - Separatrices during the Burn in the Scenarios 1, 2, 3, 5 (dashed line) and in the Steady State Scenario 4 (solid line); c - ITER Magnetic Configuration at Burn in Inductive Scenarios, Vacuum Vessel, CS, PF, TF Coils and the Locations of the 6 Controlled Gaps

Table 3.7.4-3 Plasma Parameters, Magnetic Flux Available for Burn, and Expected Duration of Burn

Scenario	**1**	**2**	**3**	**4**	**5**
I_p, MA	**15**	**15**	**13.5**	**9**	**17**
R/a, m	6.2/2.0	6.2/2.0	6.2/2.0	6.35/1.85	6.2/2.0
$\kappa_{sep}/\delta_{sep}$	1.85/0.48	1.85/0.48	1.85/0.48	1.97/0.58	1.85/0.48
κ_{95}/δ_{95}	1.70/0.33	1.70/0.33	1.70/0.33	1.85/0.42	1.70/0.33
R_{axis}/Z_{axis}, m [1)]	6.42/0.54	6.41/0.54	6.45/0.54	6.69/0.51	6.42/0.54
R_X/Z_X, m [2)]	5.09/-3.36	5.09/-3.36	5.09/-3.36	5.09/-3.35	5.09/-3.36
q_{95}	3.0	3.0	3.3	5.0	2.7
q_{axis}/q_{min}	1/1	1/1	1/1	2.8/2.4	1/1
reference l_i	0.85	0.85	0.90	0.61	0.77
min l_i/max l_i	0.7/1.0	0.7/1.0	0.7/1.0	-	0.7/0.9
β_p/β_N	0.70/1.88	0.65/1.75	0.80/1.94	1.9/3.0	0.7/2.1
$\Delta\Psi_{burn}$, Wb	37	30	53	≈10	20
Δt_{burn}, s	500	400	1000	∞	200

[1)] "axis" = magnetic axis; [2)] "X" = X- point;

The PF system has been designed to provide a sufficient degree of shaping flexibility. The CS consists of six modules. All PF coils and all CS modules, except for the two central modules, have independent power supplies, used for plasma current, position and shape control. The two central modules of the CS are, instead, connected in series to a common power supply unit.

3.7.4.1.2 Analysis of Poloidal Field Scenarios

All the scenarios mentioned above were at first studied using plasma equilibrium codes (EQUCIR[1] or TOSCA[2]) with partly prescribed plasma position and shape. The codes use prescribed values of l_i and β_p. The deviation of the separatrix from the target separatrix, shown by the dashed line in Figure 3.7.4-1b, was minimised. The assumptions on the resistive losses of the poloidal magnetic flux are given in Table 3.7.4-4.

Table 3.7.4-4 Assumptions on the Resistive Consumption of the Poloidal Magnetic Flux

Resistive flux loss at breakdown	10 Wb
Resistive flux loss during the plasma current ramp-up until SOH	$0.45\mu_0\Delta(R_pI_p)$*
Resistive flux loss from SOH to SOB for inductive scenarios	10 Wb
Resistive flux loss from SOH to SOB for hybrid and non-inductive scenarios	17 Wb
Resistive flux loss during the plasma cooling (till EOC)	10 Wb

* $\Delta(R_pI_p)$ represents variation of the parameter (R_pI_p)

Two types of studies have been performed with the above codes.

- A complete study of the operational range of l_i in order to obtain the magnetic flux available for burn, the maximum values of the (scenario) currents in the CS and PF coils, and the CATIA plasma models. Three different values of l_i (minimum, reference and maximum), shown in Table 3.7.4-3, were considered for scenarios 1, 2, 3 and 5 at SOH, SOF, SOB and EOB. For scenario 4 only, plasma with reference values of l_i was analysed. The magnetic flux available for burn in these scenarios (reference l_i) is given in Table 3.7.4-3. The table also shows the expected duration of the burn, assuming the appropriate plasma loop voltages in each case. The maximum value of the total flux swing of the PF system is about 280 Wb (17 MA scenario 5). The maximum values of the coil currents and of the magnetic fields at SOD and in the l_i survey at SOH, SOF, SOB, EOB states, are within the coil capabilities with some margins left for plasma control actions.
- A design of all PF scenarios in terms of plasma equilibrium snapshots. The goal was to provide the time evolution of all plasma parameters (e.g. major and minor radii, elongation, triangularity) and of the coil currents, voltages and power for the design of other systems (i.e. the power supplies).

PF scenario 2 was verified and simulated with a free-boundary time evolution plasma equilibrium code MAXFEA. This code takes into account eddy currents in the vacuum vessel and the models of power supplies. Moreover, the code simulates the feedforward and feedback control of the plasma current, position and shape, according to the control scheme described in 3.7.4.1.3. However, the evolution of l_i, β_p and the resistive flux loss needs to be

[1] H.Ninomiya, K.Shinya, A.Kameari, "Optimization of Currents in Field-Shaping Coils of a Non-Circular Tokamak", Proceedings of the 8th Symposium on Engineering Problems of Fusion Research, (1979), p.75

[2] H. Ninomiya, A. Kameari and K. Shinya; report: JAERI-M 9127 (1980). K. Shinya and H. Ninomiya; report: JAERI-M 9278 (1981). K. Shinya and S. Nishio; report: JAERI-M 87-133

prescribed as inputs in this analysis. The waveforms of the plasma parameters and of the coil currents obtained with EQUCIR were used as reference in MAXFEA simulations.

The PF system operation and the plasma evolution in scenario 2 and in scenario 4 were self-consistently simulated with the DINA[1] code, using feedback and feedforward control of the plasma current, position and shape. In addition to the MAXFEA capabilities, DINA calculates the evolution of the plasma temperature and current profiles (i.e. l_i, β_p and the resistive flux loss). The evolutions of the plasma density, Z_{eff}, and the power of the additional heating and non-inductive current drive are prescribed as inputs in this analysis. Control of the plasma current, position and shape was performed with the "JCT/February 2001" controller described in 3.7.4.1.3. DINA simulations based on the studies of these scenarios performed with the transport code ASTRA (see 4) and with the plasma equilibrium codes (EQUCIR or TOSCA).

The inductive scenario 2 was simulated in two variants: the nominal scenario and a scenario with accelerated transient phases (before and after driven burn). To check the capability of the PF system to operate in the presence of large-scale recoverable disturbances, simulations of scenario 2 with nominal transient phases were also repeated with minor disruptions (see 3.7.4.1.3). As an example, Figure 3.7.4-2 shows results of the simulation of scenario 2 with the nominal ramp-up of the plasma current (100 s) and two minor disruptions incurred at 60 s (current ramp-up) and 140 s (driven burn).

The waveforms of plasma current, minor radius, κ_{sep}, β_p, l_i, and total power required for the PF system are shown in Figure 3.7.4-2a. The positive peak of the total power is less than 100 MW. Deviations of the controlled gaps relative to their reference values are shown in Figures 3.7-2b. The deviations of all gaps during the plasma current ramp and early part of flat top are well within acceptable limits. The value of deviations is less than 40 mm.

[1] Khayrutdinov, R., Lukash, V., "Studies of plasma equilibrium and transport in a tokamak fusion device with the inverse-variable technique", J. Comput. Phys. 109 (1993) 193

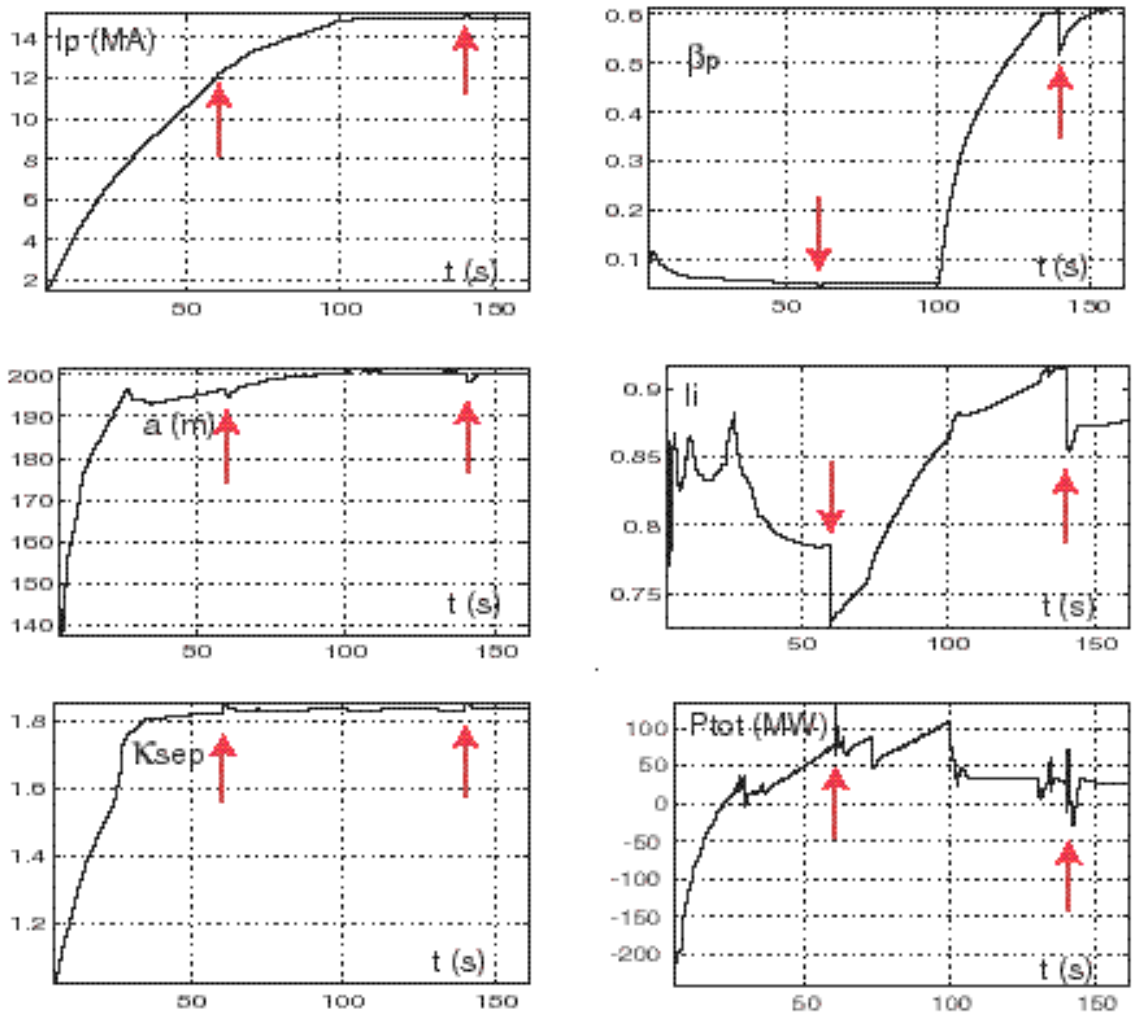

Figure 3.7.4-2a DINA Simulation of Scenario 2 with minor disruptions (see below) at 60 s and 140 s (arrows)

Waveforms of plasma parameters and total coil power

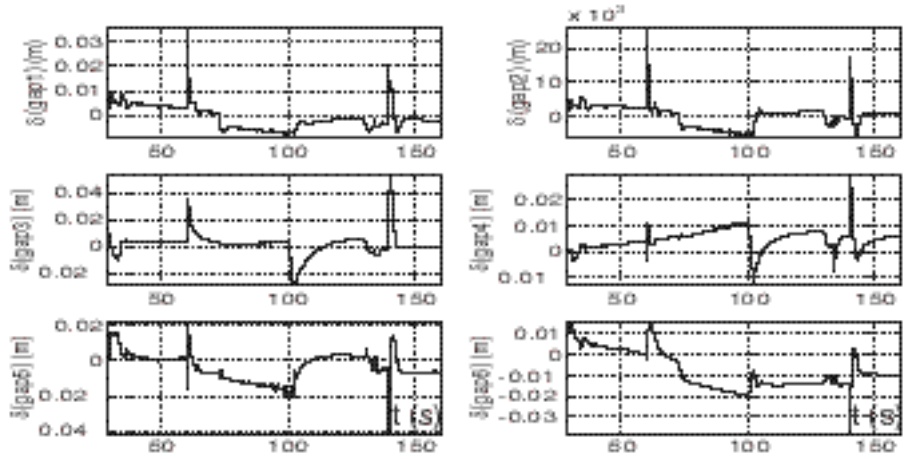

Figure 3.7.4-2b DINA Simulation of Scenario 2 with minor disruptions at 80 s and 140 s

Deviation of the controlled gaps relative to their reference values
(see comments on the signs of the gap deviations in Figure 3.7.4-5)

The plasma current ramp-up and the driven burn in the steady state scenario 4 were also simulated with the DINA code in two variants. In the first variant inductive control of the plasma current is continued till the end of the simulation (300 s). Only 9 Wb of magnetic flux is required to sustain a driven burn with 9 MA plasma current for3000 s. In the second variant the control of the plasma current by the PF system is switched off at 60 s. This leads to a plasma current reduction, over about 150 s, from 9 MA to the steady state value of 8 MA. At steady state the value of Q is 5.5 and the loop voltage is zero. The plasma current ramp-up rate in scenario 4 is higher than that in scenario 2. The positive peak of the total power is about 120 MW, higher than in scenario 2.

Studies of plasma initiation and verification of the assumptions used in the studies presented above (i.e. the magnetic flux at breakdown) were performed by simulations which take into account eddy currents in the conducting structures, plasma displacements, models of the power supplies, plasma ionisation and transport. The analysis was done with the set of the switching network resistors considered in the power supply design (see 3.4). Several codes were used in this study: the 2D electromagnetic code TRANSMAK with the 0D transport code SCENPLINT and the 2D electromagnetic code BDOS[1]. 3D electromagnetic analysis was also provided (effect of the vacuum vessel ports and ferromagnetic inserts on plasma initiation). The studies have shown the capability of the PF system to provide outboard plasma initiation, starting from 45% to 100% of the maximum magnetic flux at SOD and assuming 2 MW of EC power is transferred to the electrons.

To summarise, all the scenario studies mentioned above have demonstrated the capability of the PF system to support the scenarios 1-5 with the limits imposed on the coil currents, voltages and total power.

3.7.4.1.3 Plasma Current, Position and Shape Control

The ITER elongated plasma would be vertically unstable without the use of an active feedback control system. The double shell (each 60 mm thick) stainless steel vacuum vessel, shown in Figure 3.7.4-1c, provides the main contribution to the stabilisation of plasma vertical displacements. Important elements of the plasma passive stabilisation are also the toroidally continuous rings (stainless steel, 60 mm thick) attached to the blanket module triangular supports (shown in Figure 3.7.4-1c above the outboard divertor region). The total toroidal resistance of the vacuum vessel with the stabilising rings is 7.4 μΩ. These stabilising rings improve the up/down symmetry of the conducting structures as they couple well with any plasma vertical motion and in particular render the passive structure more symmetric with respect to the plasma. They in fact decrease the initial values of the plasma vertical displacement after a plasma disturbance by about a factor of 2. As far as the instability growth rate is concerned, the contributions to the plasma stabilisation force (participation factors) from the different conducting elements are shown in Table 3.7.4-5.

[1] "Optimizing voltage wafe forms of poloidal field coils at the plasma breakdown", I. Senda, et al., JAERI-Tech 96-016, Japan Atomic Energy Research Inst., Itaraki (1996)

Table 3.7.4-5 Participation Factors (%) of the Vacuum Vessel (Inner and Outer Shells), Stabilising Rings and Coils in Passive Stabilisation of the Plasma Vertical Displacements (Scenario 2 with $l_i = 0.85$)

State	VV inner shell	VV outer shell	Stabilising rings	CS and PF coils (each coil is short circuited)
SOF	54.8	27.1	11.7	6.4
SOB	52.6	27.4	11.2	8.8

One interesting feature of the design is that the quasi-symmetrical configuration of the PF coils (see Figure 3.7.4-1c) allows the use of one AC/DC converter, dedicated to plasma vertical stabilisation (VS), which is connected to the coils PF2 - PF5, as shown in the simplified schematic of Figure 3.7.4-3. Compared to the main AC/DC converters connected in series with each coil, the VS converter has a higher output voltage and shorter response time. The on-load voltage limit of the VS converter is 6 kV. The on-load voltage limit of the CS and PF coil converters (main converters) is set at 1.5 kV, except for the one driving the CS1U and CS1L coils (the coil modules nearest the machine mid-plane) connected in series, which is set at 3 kV. The VS converter carries only the imbalance current, which is the algebraic sum of the currents in the coils PF2 through PF5. The scenario value of the imbalance current is typically limited to 12 kA, while the total admissible value is 22 kA.

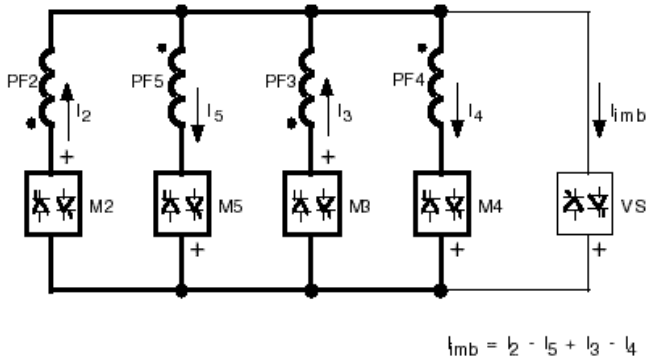

Figure 3.7.4-3 The Vertical Stabilisation Circuit

For an optimal use of these features, a control scheme with two feedback loops acting on different time scales has been designed and is schematically shown in Figure 3.7.4-4. In the fast VS loop, the feedback algorithm determines the voltage of the VS converter using as input the vertical velocity of the plasma current centre. Its identification, performed by magnetic diagnostics, is simulated with a first order transfer function with 3 ms time constant. The slow feedback loop provides control of plasma current and shape by acting on the CS and PF coil main converters. Plasma shape control in divertor configurations is realised with the control of the six gaps between the separatrix and the plasma-facing components (the first wall and the divertor) shown in Figure 3.7.4-1 (c). Figure 3.7.4-4 shows the transfer functions of the various components present both in the fast loop and in the slow loop. Current and shape identification, performed again by magnetic diagnostics, is simulated with a longer time constant, 150 ms.

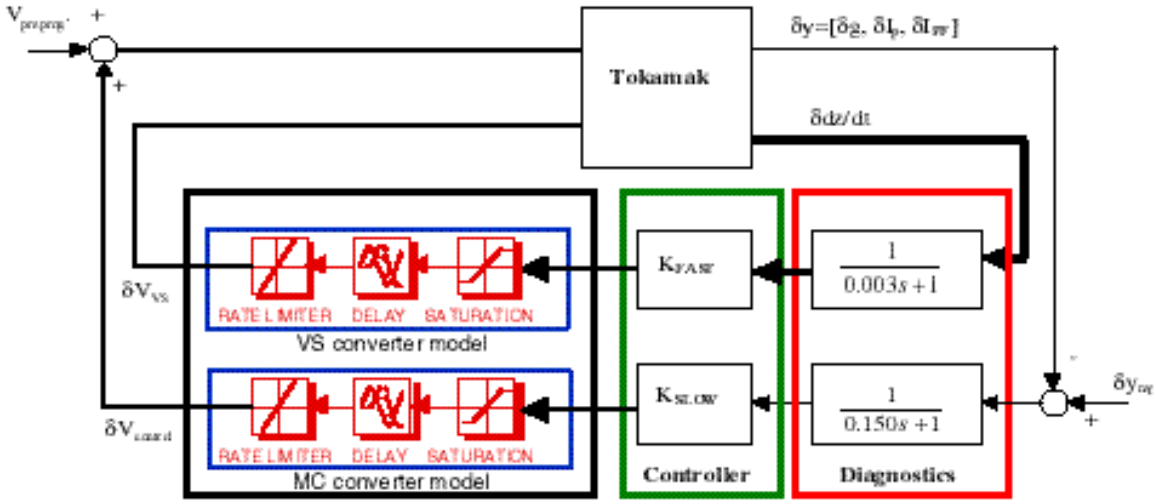

Figure 3.7.4-4 Plasma Current, Position and Shape Control
A two loop control scheme is adopted
(fast loop for vertical stabilisation shown in bold arrows)

The resulting closed loop bandwidth of the fast loop is about 20 rad/s, whereas the slow loop bandwidth is about 1 rad/s; the two loops are therefore well decoupled in the frequency domain.

Two types of large-scale recoverable plasma disturbances, minor disruptions (MD), are used for the design of the controllers and for their studies in the inductive scenarios.

- MD1: an instantaneous l_i drop of 0.2 (l_{i0} – 0.5) without recovery, simultaneous with a β_p drop of 0.2 β_{p0} followed by 3 s exponential recovery.
- MD2: an instantaneous β_p drop of 0.2 β_{p0} followed by 3 s exponential recovery.

The corresponding instantaneous variation of the plasma current is calculated assuming conservation of magnetic helicity.

Several controllers have been designed on the basis of the linear, non-rigid plasma displacement model derived from the PET code. Several controllers for the divertor phases were analysed. The "RF/April 2001" controller design uses the linear quadratic Gaussian (LQG) approach for both the fast and the slow feedback loops. The "JCT/February 2001" controller design combines the LQG VS controller with the LQG controller for the plasma current and shape. The "EU/April 2001" controller design combines a lead network VS controller with two separate decoupling controllers for plasma current and shape, including integral actions to eliminate the static errors. The controllers were used to simulate minor disruptions in the key states of the scenarios described in 3.7.4.1.1. Different possible strategies for controlling the plasma during the limiter phase were also investigated. Various types of these controllers were designed, differing in the set of controlled variables and in the design technique.

Linear plasma models were used for design of the controllers and for preliminary analysis of the controller performance in the case of minor disruptions. Figure 3.7.4-5 shows, as an

example, waveforms of gaps, coil currents, voltages and power in the simulation of plasma current, position and shape control during an MD1 (scenario 2, SOF, $l_i = 0.85$).

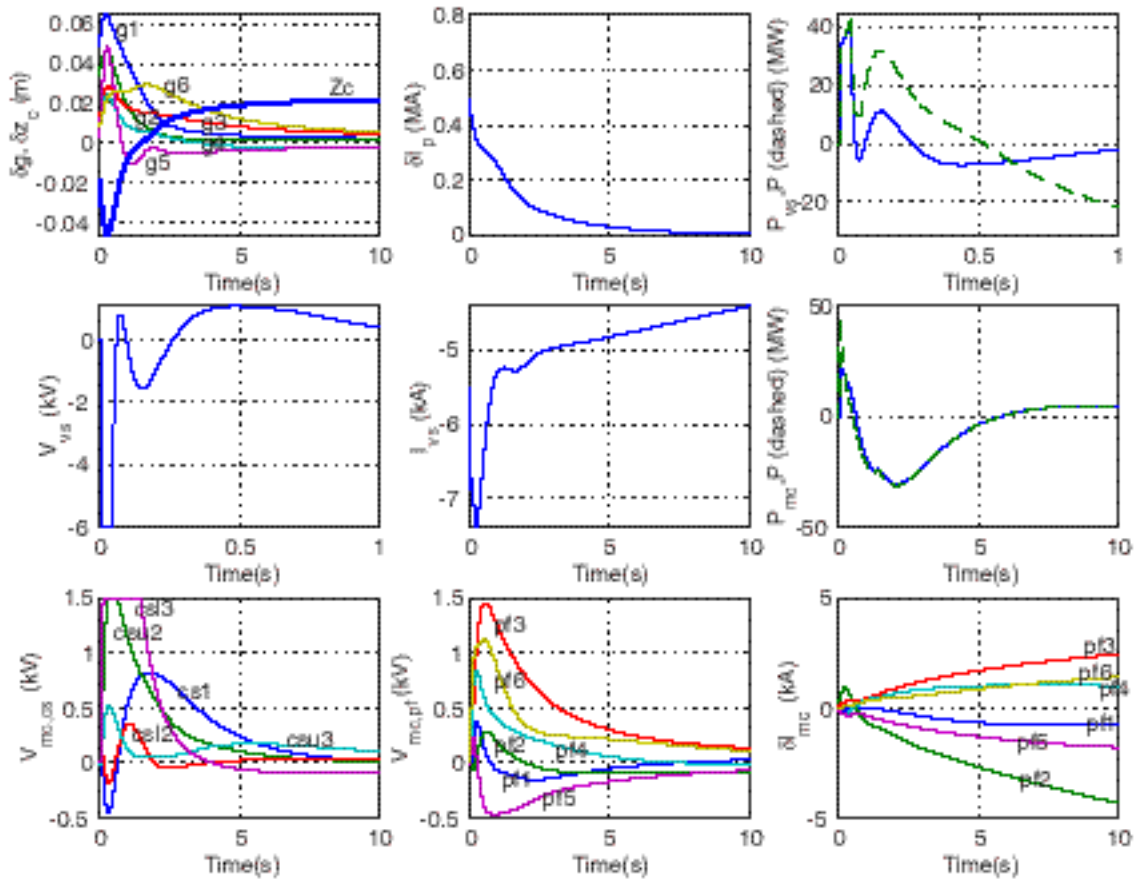

Figure 3.7.4-5 Plasma Current, Position and Shape Control during MD1 in Scenario 2 (SOF, $l_i = 0.85$). Linear model derived from PET code, "JCT/February 2001" controller

δg – deviation of the gaps from the reference values, δz_c – displacement of the current centroid from the reference value, δI_p – variation of plasma current, P - total active power, V_{VS}, I_{VS} and P_{VS} – voltage, current and power of the VS converter, V_{mc} – voltage of the main converter, δI_{mc} – variation of current in the main converter.

Positive g1 and g2 deviations correspond to displacement of the separatrix legs towards the divertor dome. Negative g3 – g6 deviations corresponds to decrease of the gap between the separatrix and the first wall.

Similar simulations were provided for the key states of scenarios 1, 2, and 5 with the various plasma equilibria having different l_i. Both minor disruptions (MD1 and MD2) were considered during the burn. The studies were done with the controllers described above. The main results of the linear model simulations can be summarised as follows. The settling time of the gap control, defined as the time needed for the deviation of all the gaps to become less than 10 mm, is about 5-20 s. The maximum displacement of gap 1 (inner separatrix leg) towards the divertor dome is within 100 mm. In a few cases, the separatrix inner leg slightly interacts, during a minor disruption, with the divertor dome (by less that 20 mm for less than 5 s), but these plasmas have low β_p. The maximum displacement of gap 2 (outer separatrix

leg) is within 70 mm, which does not lead to interaction of the outer separatrix with the dome. For controllers having a settling time for plasma shape control of 5-10 s, the maximum displacement of the separatrix towards the first wall is about 30 mm for gaps 3 and 4, whereas for gaps 5 and 6 it is about 90 mm. These values are within the acceptable limits.

The "EU/April 2001" controller has been also validated in simulation on the linear model including the plasma shape reconstruction algorithm in the feedback loop and taking into account the effects of noise on the magnetic flux and field measurements.

The overall performance of the shape control has been found to be satisfactory. However, the relatively high plasma elongation with its short growth time implies peak power requirements, of about 100 MW (positive active power). Moreover, the largest power steps found in the simulations with the linear models are of about 90 MW. A preliminary study of the power management system was provided with the goal to reduce the power steps. The system is based on the possibility of transferring electrical power from one coil to other coils. In addition to the linear plasma models, the MAXFEA, PET and DINA free plasma boundary time varying codes have been used in order to analyse the performance of the controllers (see, for example, the results presented in Figure 3.7.4-2).

Possible abnormal operational regimes, due to failure of one PF converter or current saturation in one PF coil, were also studied at a preliminary level. The analysis concludes that in all key states of scenario 2 the "EU/October 2000" controller is able to counteract a minor disruption and restores the plasma shape in 20 s, even if one of the PF converters fails (produces zero voltage). The shape control accuracy is affected by the failure but the controller limits the plasma wall interaction to reasonable values. A strategy to counteract the possibility of current saturation in the PF coils was also developed. An anti-saturation controller, changing the reference signals for the gaps, was proposed. The simulations performed with such a device, both on linear and non-linear models, show the effectiveness of such a system in keeping the coil currents far from their saturation limits with a moderate deterioration on the shape control accuracy.

Several studies were done to estimate the effect of the vacuum vessel ports and other conducting structures on the plasma current, position and shape control. The results can be summarised as follows. The vacuum vessel ports decrease the growth time of plasma vertical instability by 10-20%. The blanket modules have deep cuts in the poloidal direction which, for a model with five plasma facing slits, decreases the eddy current decay time to about 2 ms. This leads to an insignificant effect of the blanket modules on the plasma vertical stabilisation. The TF intercoil structures, the cryostat and the outer-cryostat structures affect insignificantly the plasma current, position and shape control.

3.7.4.1.4 Error Fields, Correction Coils and RWM Stabilisation

Error Fields

Error fields (any perturbation of the axial symmetry of the magnetic field) can drive the formation and growth of locked modes in otherwise MHD-stable plasmas. The most critical

period for the locked modes is the last phase of the current ramp-up when the plasma density is low. Recent experiments in DIII-D[1] have also shown that correction of the error field allows the plasma rotation to be maintained above the threshold for rotational stabilisation of the resistive wall mode (RWM).

The following "3-mode" error field criterion has been adopted for the ITER design:

$$B_{3-\mathrm{mode}}/B_0 = \sqrt{(B_{2,1}/B_0)^2 + 0.8(B_{3,1}/B_0)^2 + 0.2(B_{1,1}/B_0)^2} \le 5 \times 10^{-5},$$

where $B_{1,1}$, $B_{2,1}$ and $B_{3,1}$ are the amplitudes of the (1,1), (2,1) and (3,1) modes of the normal component of the non-axisymmetrical magnetic field to the q = 2 surface, and B_0 is the value of toroidal magnetic field (5.3 T), at R = 6.2 m.

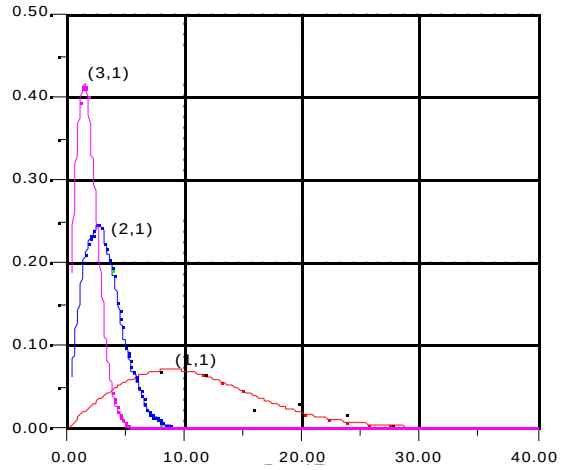

$B_{m,1} / B_0$ (in 10^{-5})

a

Probability Density of (m,n) = (1,1), (2,1) and (3,1) Error Field Mode Amplitudes.

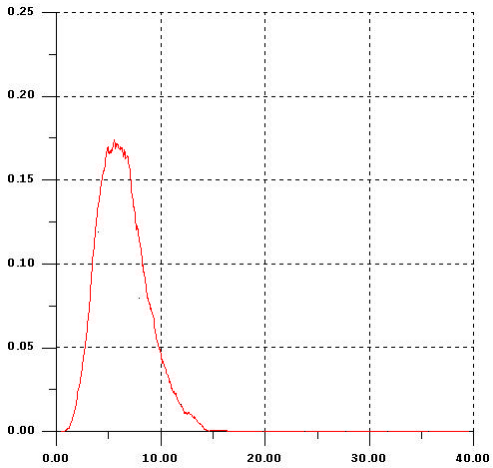

$B_{3\text{-mode},1}/B_0$ (in 10^{-5})

b

Probability Density of 3-mode Error Field Amplitude.

Figure 3.7.4-6 Error Fields from CS, PF and TF Coils Misalignment at SOF in scenario 2

The misalignments of the TF, CS and PF coil current centrelines, arising during the coil manufacture, installation and assembly, are the main contributors to the error field. A tolerance analysis has been used to estimate the deviation of the coil centrelines from their nominal position and shape. The expected error fields have been calculated with Monte-Carlo simulations using the various degrees of freedom in the coils deviation. A uniform distribution of these deviations, within the limits resulting from the tolerance analysis, was assumed. The probability density of the error field modes expected at SOF in scenario 2 is shown in Figure 3.7.4-6. From Figure 3.7.4-6b the expected "3-mode" error field is less than 9.5×10^{-5} with probability 90% and less than 15×10^{-5} with probability 99.9%.

[1] DIII-D Weekly Reports, 2001

Additional error fields are produced by the neutral beam magnetic field reduction system (NB MFRS) and by ferromagnetic materials used in the Test Blanket Modules (TBM). The "3-mode" error field due to the NB MFRS (two NB injectors and the diagnostic injector) is about 1.1×10^{-5}, whereas five TBMs, having the ferromagnetic material, produce 3.1×10^{-5}.

Correction Coils

A correction coil (CC) system has been designed for ITER to bring the above-mentioned error field down to an acceptable level. The CCs (shown in Figure 1.4.1-3) consist of three sets of superconducting coils (top, side and bottom) distributed poloidally to provide control of poloidal fields with several m mode numbers. Each coil is connected to the opposite coil in anti-series, to produce an n = 1 asymmetric mode and to avoid coupling with axisymmetrical magnetic fields. Three power supplies are used for each CC set to provide toroidal directionality for the error field components. The CC current limits based on the requirements and on the design consideration are: 140 kAt for the top coils, 200 kAt for the side coils and 180 kAt for the bottom coils.

Currents in the CC required to correct the total error fields from the three NB MFRSs and from the five TBMs are as follows: 8 kAt in the top CC, 20 kAt in the side CC and 16 kAt in the bottom CC. A Monte-Carlo simulation has shown that, with a probability of 99%, the rest of the CC currents, available for the correction of other error fields, are sufficient to reduce the error field anticipated from the CS, PF and TF coils to the design criterion of 5×10^{-5}. The top and side CCs have margins in the currents for this error field correction: about 20 kAt in the top CC and about 55 kAt in the side CC. The margin in the current of the side coils is important also for active stabilisation of the resistive wall modes (RWM).

RWM Stabilisation

The main approach to steady state operation in ITER is via a weak or negative central magnetic shear, high-bootstrap-current discharge. In the absence of a nearby conducting wall, such discharges are unstable to the n = 1 external kink mode at $\beta_N \approx 3$ (due to the low value of l_i), while equal or larger values of β_N are needed to achieve Q = 5. When a resistive (i.e. not perfectly conducting) wall is present, these modes are no longer ideally unstable but can develop RWMs, which grow on the time scale of the magnetic field penetration through the wall, τ_w.

Detailed studies of RWM stabilisation in ITER have not been performed. However, an estimate of the requirements for the currents and voltages in the side CCs was made. A 3D electromagnetic model (without plasma) was used in the analysis. The penetration time of the CC magnetic field through the vacuum vessel was estimated to be about 0.3 s. This time defines the frequency of the CCs currents required for the stabilisation, i.e. about 2 Hz. A 20 kAt current is required for the side CCs to produce, at this frequency, a radial magnetic field of about 1 mT inside the vacuum vessel (several times above the level of detection of the RWM). 13 V/t is required for the side CCs to provide this current amplitude at the 2 Hz frequency, assuming that the single turn inductance of a pair of coils is 50 $\mu H/t^2$.

Parameters of the ITER power supply, chosen for the side CC, can be compared with the AC capability of the new power supply of C-coils used in the DIII-D for RWM stabilisation[1]. The DIII-D power supply has frequency $f = 100$ Hz with maximum current $I = 5$ kAt. Taking into account the position and size of the DIII-D C-coils normalised by the plasma minor radius, which are then very similar to the ITER side CCs, parameters for the ITER power supply can be scaled from the corresponding DIII-D parameters as follows:

$$f(ITER) = f(DIII-D) \times \frac{\tau_w(DIII-D)}{\tau_w(ITER)}, \quad I(ITER) = I(DIII-D) \times \frac{I_p(ITER)}{I_p(DIII-D)}.$$

Substituting τ_w(DIII-D) = 5.8 ms, τ_w(ITER) = 300 ms, I_p(DIII-D) = 1.5 MA, I_p(ITER) = 9 MA (scenario 4), one obtains for the ITER power supply the frequency 1.9 Hz and the current 30 kAt. These values are consistent with the power supply parameters chosen for the ITER side CC.

3.7.4.2 Kinetic Control

3.7.4.2.1 Kinetic Control Requirements in ITER

Tokamak plasma control encompasses both magnetic configuration control, covered above, as well as kinetic control. There is a clear distinction between magnetic control and kinetic control in terms of the actuators used (the PF coil system is used for magnetic control whereas heating, fuelling and pumping systems are used for kinetic control). In this section, kinetic control in the inductive operation is mainly described although many of the issues are also relevant to steady state operation. Current profile control in the start-up phase is also investigated in its relation to MHD stability.

At the simplest level, the key kinetic attributes of the core plasma control are density, temperature, impurity content, current density, and fusion power. The key attributes of the divertor plasma control are density, temperature, impurity content, radiation power in the core and the divertor region, and the power to the divertor target. Among these attributes, the most important attributes to be controlled are fusion power P_{FUS} and the power to the divertor target plates $P_{Divertor}$. In addition also the power P_{LOSS} across the edge pedestal region should be controlled for the transition from L- to H-mode (in the start up phase) and H- to L-mode (in the shutdown phase).

To control the above three variables (P_{FUS}, $P_{Divertor}$ and P_{LOSS}), there are four main actuators; 1) additional heating power P_{ADD}, 2) DT gas or pellet injection rate, 3) high-Z impurity (for example, argon) injection rate, and 4) pumping rate.

The control system is non-diagonal as every input variable has an effect on every desired output. However, the strongest effect on fusion power is given by changing the particle density. Additional heating has a major impact on both fusion power and L-H transition control, whereas heavy impurity injection has its main impact on the local radiated fraction in the divertor region.

[1] A.M. Garofalo et al., Nucl. Fusion 40 (2000) 1491

3.7.4.2.2 Kinetic Control in the Reference Inductive Scenario

Fusion Power and Divertor Power Control in the case of Sudden Increase of Confinement Time

The dynamic response of the fusion power to internal (plasma-induced) perturbation is an important issue. Modelling of the plasma burn dynamics with a time-dependent simulation model provides insight into both the inherent response of the plasma and the effectiveness of various burn control systems.

Figure 3.7.4-7 shows a simulation of the response of the power control system to a hypothetical plasma disturbance in which a sudden change of energy confinement occurs. Confinement enhancement factor $H_{H98(y,2)}$ is increased by 20% during the current flat top (t = 300 s) in the reference scenario. The electron density $\langle n_e \rangle$ is controlled to keep the fusion power constant. By controlling argon impurity fraction, the power to the divertor region is also maintained at 30 MW, which approximately corresponds to 5 MWm^{-2} heat load on the target. This analysis also shows that the direct use of fuelling control, for example by cutting back the fuel injection rate, is an effective method in limiting fusion power excursions.

Control of Fusion Power in High-Q Operation by Impurity Seeding

The control of fusion power excursion is one of the most important issues in the fusion reactor. In the case of high-Q or ignited operation, fusion power can not be controlled only by the additional heating power. In this case, high-Z impurity seeding or density control has been considered as one of the means for burn control.

Figure 3.7.4-8 shows a simulation where the suppression of the fusion power excursion is achieved by impurity injection. Here, I_P = 17 MA, $\langle n_e \rangle = 1.18\times10^{20} m^{-3}$ ($\langle n_e \rangle / n_G = 0.87$), $\tau_{He}^*/\tau_E = 3$, $H_{H98(y,2)} = 1.0$ and, as an artificial disturbance, a heating power P_{ADD} is added from 10 s to 13.7 s. The dotted line denotes the case without impurity seeding. In this case, a large overshoot of fusion power is observed. In the case of the solid line, argon impurity (Ar) is injected and the overshoot of fusion power is suppressed.

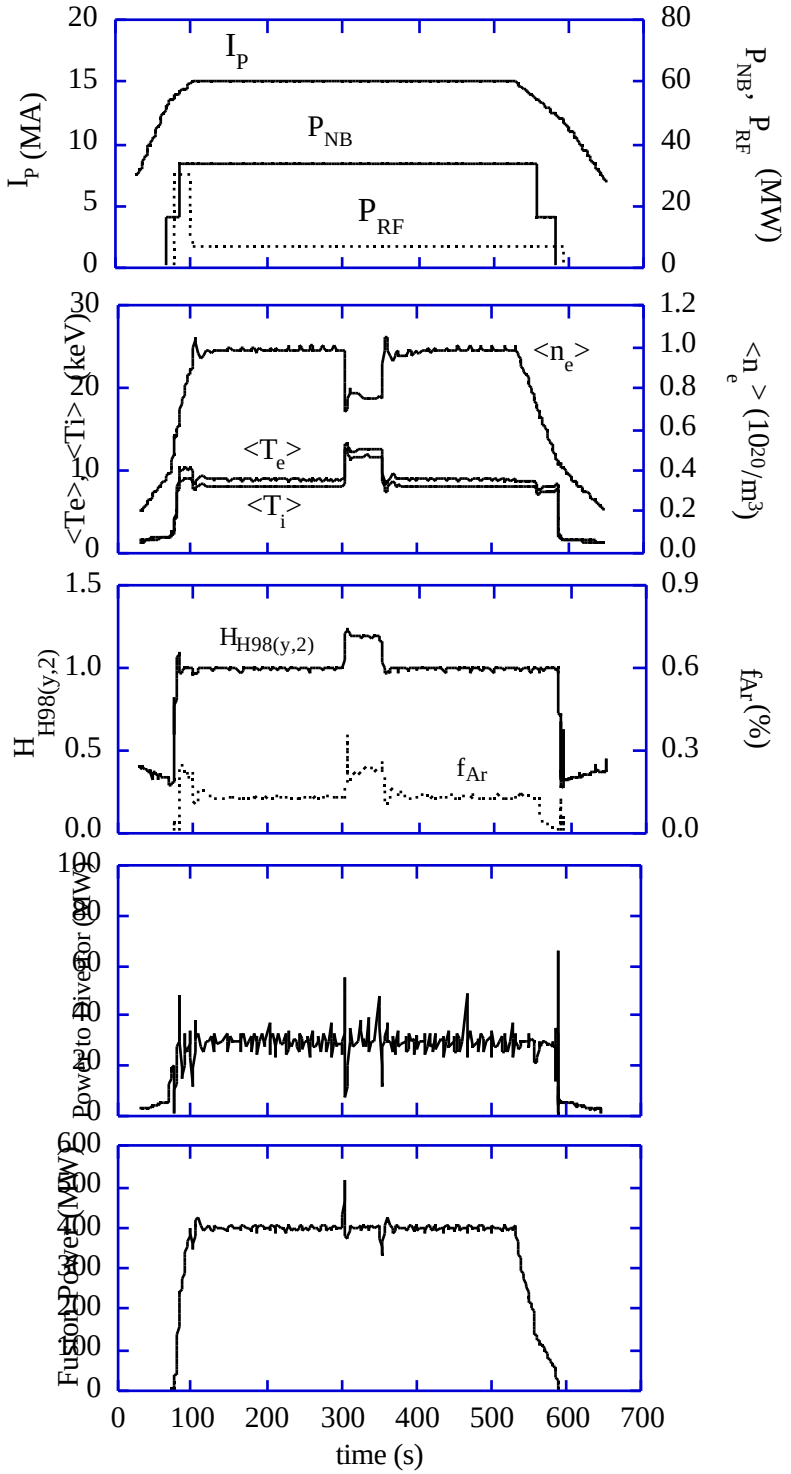

Figure 3.7.4-7 Fusion Power Control by Density Control in case of Sudden Increase of Energy Confinement Time

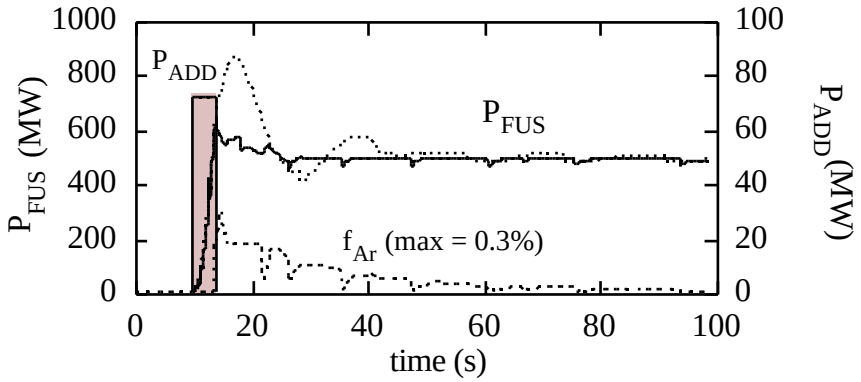

Figure 3.7.4-8 Suppression of Fusion Power Excursion by Impurity Seeding in Ignited Operation

Here, I_P = 17 MA, τ_{He}^*/τ_E = 3, $H_{H98(y,2)}$ = 1.0 and 73 MW of additional heating power (P_{ADD}) is added from 10 s to 13.7 s.
solid line: with argon (Ar) impurity seeding, dotted line: without impurity seeding

3.7.4.2.3 Control of Current Profile in Start-up Phase

In the start-up phase, the current profile can be modified by changing the current ramp-up rate and/or the timing of the heating. In this case, magnetic control and kinetic control are linked to each other.

Figure 3.7.4-9 shows various start-up scenarios of ITER. Cases (a) and (b) are with heating after current flat-top, and case (c) is with heating during current ramp-up. In cases (b) and (c), the current ramp-up rate is reduced by a factor of 2 at the final stage of current rise. It is seen that the plasma internal inductance $l_i(3)$ increases by decreasing the current ramp-up rate. Higher $l_i(3)$ indicates a more peaked current density profile.

The figures on the bottom row show the trajectory in q_{95}-$l_i(3)$ space. X-point formation (XPF), start of heating (SOH), start of flat-top (SOF), start of burn (SOB), end of burn (EOB) and end of cooling (EOC) are shown. Dotted lines show the empirical stability boundary. The trajectory in q_{95}-li(3) space can be controlled by the start time of the additional heating.

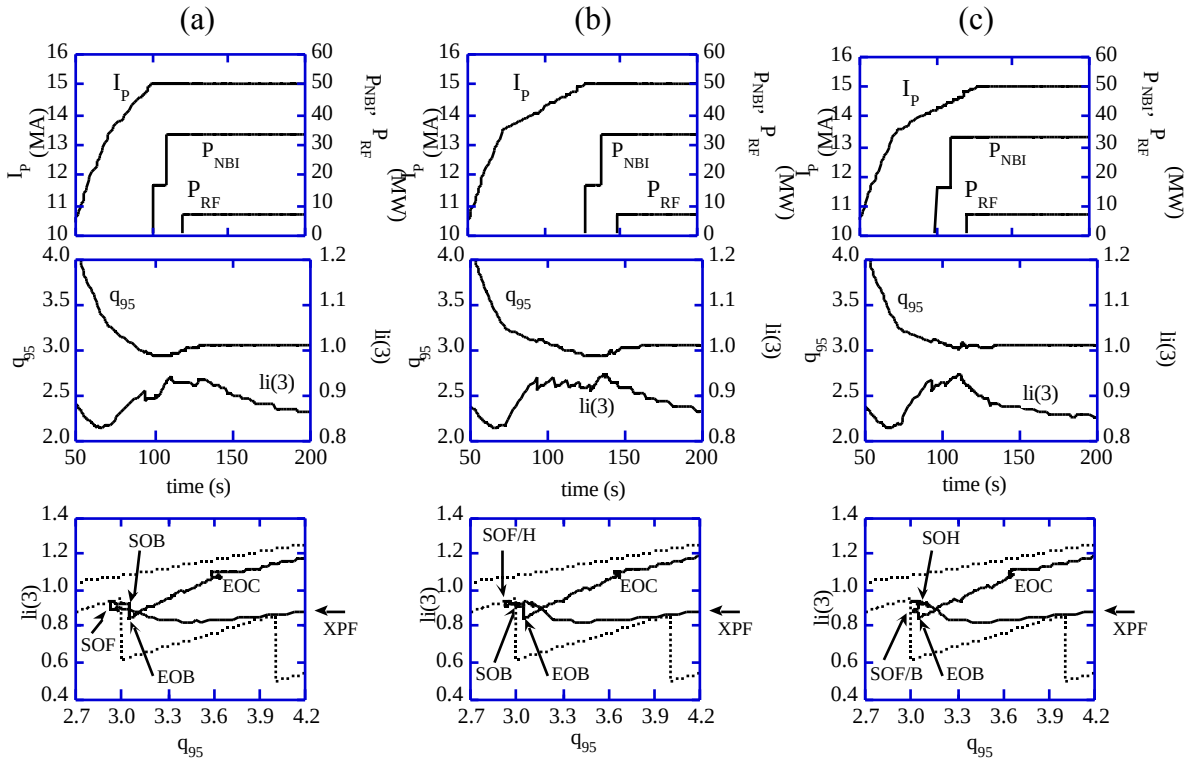

Figure 3.7.4-9 Various Start-up Scenarios
(a) and (b) with heating after current flat-top, (c) with heating during current ramp-up

3.7.4.2.4 Control of Magnetic Shear and ITB Formation from Conventional q-profile

In non-inductive operation, current profile control is an important issue. Figure 3.7.4-10a shows a demonstration of ITB (internal transport barrier) formation from a conventional q-profile by using a simple model in which an ITB is formed when magnetic shear rq'/q is < 0. Here, I_P = 9 MA and $\langle n_e \rangle = 0.67 \times 10^{20} m^{-3}$. Starting from a normal shear plasma ($P_{FUS}/P_{NB}/P_{RF1}$ = 140 MW/20 MW/20 MW), peripheral current drive (P_{RF2} = 40 MW) is added at t = 300 s. An ITB is formed at 640 s and steady state conditions with Q = 3.5 (P_{FUS} = 280 MW) are obtained at about 2000 s. Here, current drive efficiencies assumed are $\gamma_{20}(NB) = 0.18 - 0.28$ and $\gamma_{20}(RF2) = 0.3$. Figure 3.7.4-10b shows plasma profiles corresponding to a). Here, the RLWB transport model[1] is assumed. Thermal diffusivity χ (and also particle diffusivity) is reduced to the neo-classical level at r/a < 0.7 where magnetic shear rq'/q < 0. A large current drive power (~ 40 MW) in the peripheral region is required in addition to 40 MW of on-axis (RF) and off-axis (NB) current drive.

For the non-inductive operation mode, time response of plasma parameters to various perturbations (confinement, impurity fraction, current drive power, pumping speed and fuelling rate) has been investigated. Current penetration determines the rate of profile changes and the time constant of any plasma parameter is usually longer than 100 s.

[1] D. Boucher, et al., in Proc. 16th IAEA Fusion Energy Conference, Montreal, 1996 (IAEA,Vienna, 1997) 945

a)

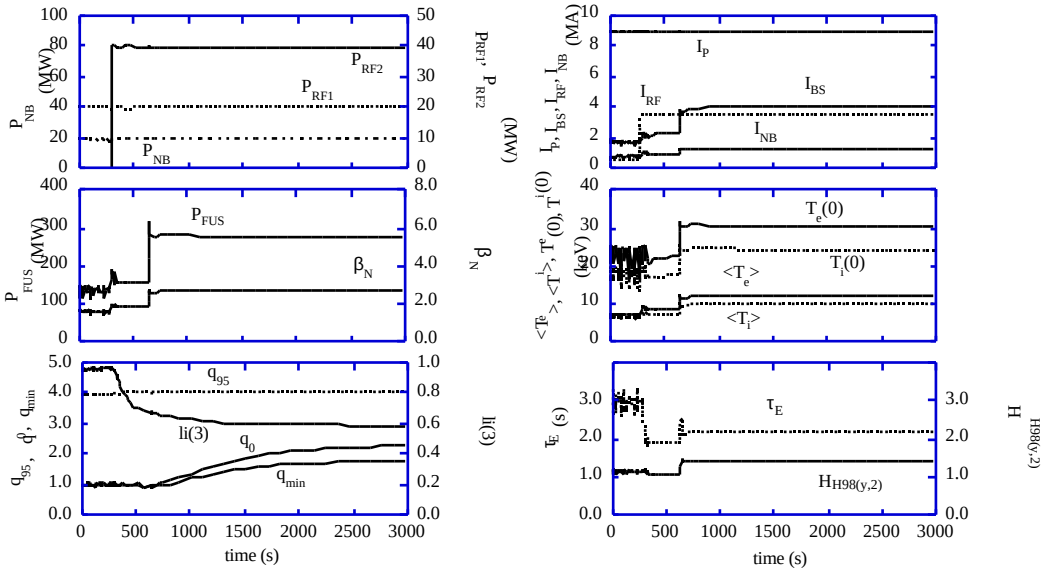

b)

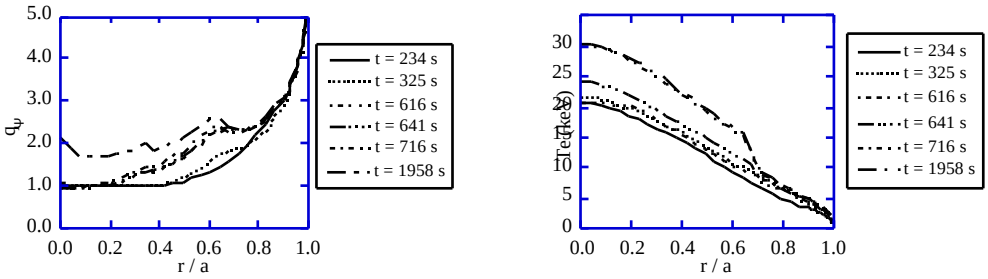

Figure 3.7.4-10 ITB Formation from a Conventional q-profile

a) Time histories of current drive powers (P_{NB}, P_{RF1}, P_{RF2}) and plasma parameters.
b) Profiles of mhd safety factor (q_ψ) and electron temperature T_e corresponding to a)

3.7.4.2.5 Start-up Scenario in Non-inductive Operation

In this section, more realistic start-up scenario including growing plasma size is described. Here, the 1.5D transport code ASTRA[1] is used. Figure 3.7.4-11 shows the simulation result for the start-up of non-inductive operation with weak negative shear (WNS). Simulation starts from a limiter plasma with small plasma minor radius (R/a = 7.4 m/0.8 m). After plasma initialisation phase, the plasma current profile is almost flat with high central $q_o \sim 2$. Such profile is close to the desirable one at the current flat-top phase. To prevent current peaking, a fast current ramp-up rate and an additional heating power are required. For example, the average current ramp-up speed is increased to 0.25 MAs^{-1}, 6 MW of the ECRH power is applied at t = 0.1 s and then increases to 8 MW at t = 6 s. 3 MW of LH power is also applied at t = 3.5 s. At this limiter phase, the input power is kept smaller than the maximum limiter heat load $P_{loss} < 15$ MW. After the X-point formation (t = 15.7 s, I_p = 5 MA), the LH power is increased to 15 MW at t = 24 s, to 25 MW at t = 25 s and to 29 MW at t = 26 s to provide the L-H transition at low density and replace the ECRH power, which is switched off. One NB injector is switched on at t = 27 s, and the other at t = 28.5 s, when plasma density reaches $4\times10^{19}m^{-3}$ and shine-through losses drop to an acceptable level. Each of two

[1] G. V. Pereverzev, et al., IPP 5/42 (1991)

NB injectors (on-axis and off–axis) delivers 15 MW. The gradual replacement of carbon by argon (27 s < t < 40 s) enables reduction of the loss power from the core to the level compatible with the divertor constraints P_{loss} < 100 MW. In this scenario, the resistive voltage drops to zero in ~ 100 s. The total required flux consumption is about 5 Wb. Although a complete steady-state current profile relaxation takes about 2000 s from a conventional centrally-peaked current profile(see the previous section), an almost steady-state condition is achieved within 300 s by optimisation of the current ramp-up rate.

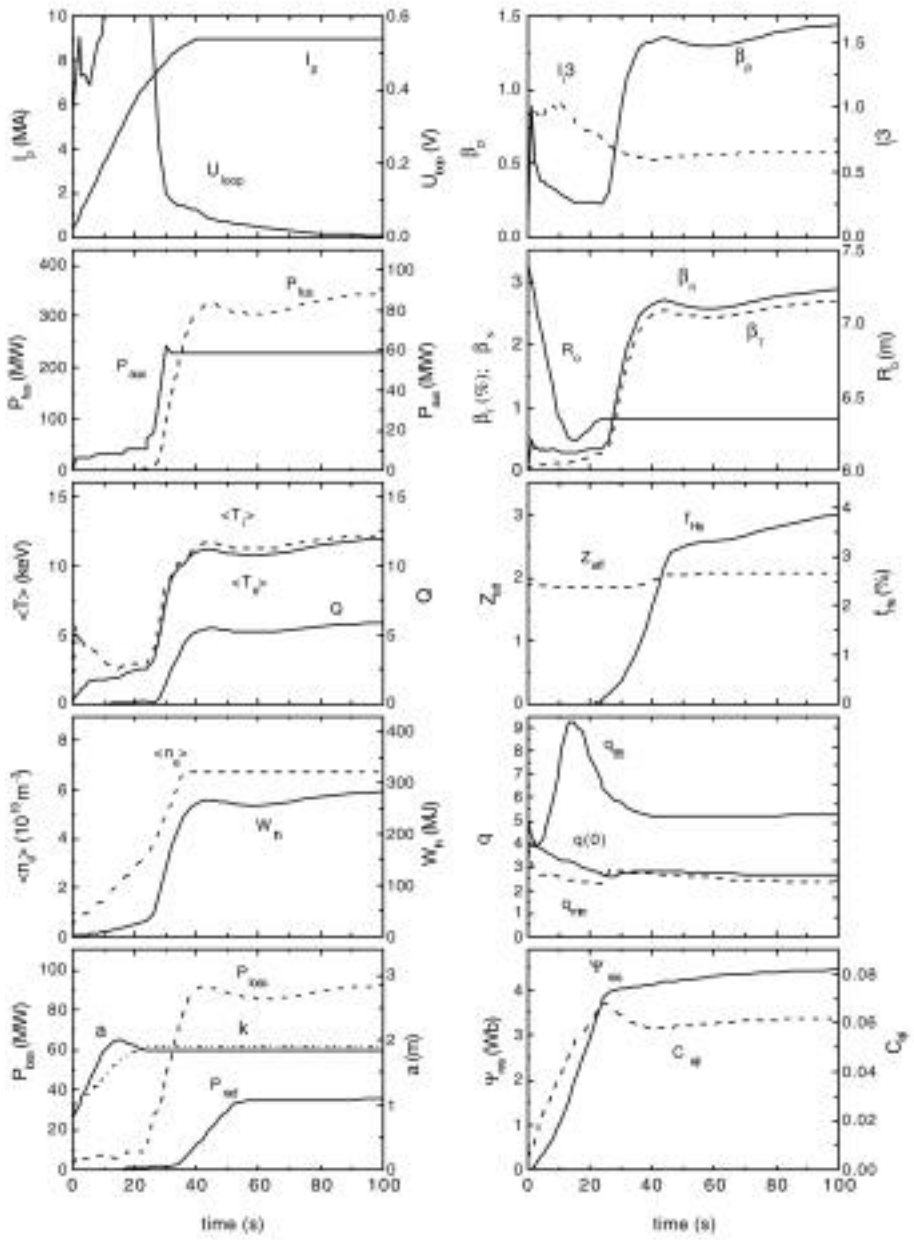

Figure 3.7.4-11 Start-up Scenario for Non-inductive Operation
X-point formation corresponds to t = 15.7 s, start of flat-top corresponds to t = 40 s and start of burn corresponds to t = 40 s.

3.7.4.2.6 NTM Stabilisation

ITER can achieve its goal of Q ≥ 10 with β_N as low as 1.5 and even at fusion power levels of 500 MW, β_N is ~ 2. Nevertheless, in present experiments with long-pulse, low collisionality plasmas, neoclassical tearing modes (NTMs) can limit β and degrade energy confinement within the range of β_N foreseen for ITER operation[1] (and well below the ideal mhd stability limit). The predominant modes are (m,n) = (3,2) and (2,1), with the former typically producing a 10-30% degradation in confinement, while the latter results in major disruptions.

Although a scatter in available data does not allow a precise scaling of critical quantities, such as the minimum seed island width, it has been found in several tokamaks that the minimum β for the onset of NTMs falls approximately linearly[2] with the normalised Larmor radius $\rho_i *$.

If this scaling is valid in the range of small $\rho_i *$, the critical β_N in ITER would be about 0.5, which is below the operational value. Since this prediction is based on limited data in the range far from ITER, and since at very low $\rho_i *$ the seed island is expected to be too small to overcome the stabilising factors (polarisation current and incomplete pressure flattening in the island), usually higher estimates for critical β_N for ITER are given[2]. However, given a large uncertainty in prediction, it is necessary to develop NTM stabilising techniques.

The growth time of NTMs is determined by the timescale for resistive reconnection in the vicinity of the relevant rational q surface, which is long enough to permit stabilisation by ECCD in present experiments[3], and should lie in the range 10–30 s in ITER. Therefore, an ECCD-based stabilisation system for NTMs will be installed to suppress (3,2) and (2,1) modes. Two possibilities have been explored computationally: (i) mode stabilisation by ECCD modulated in phase with the island O-point, and (ii) reduction in width of the saturated island by continuous ECCD. Theoretical calculations show that a modulated ECCD current density exceeding 1.5 times the bootstrap current density in the neighbourhood of the rational surface (driven in the forward direction in the island O-point) will stabilise an arbitrarily small island.

Initial analyses of power requirements have shown that (3,2) and (2,1) NTMs could be stabilised (individually) in a time of order 10 s by 10-30 MW of modulated ECCD power[4] in devices of the ITER class (see Figure 3.7.4-12). There is a satisfactory agreement between different approaches. The scatter in the predictions is partly related to the island detection size. For example, an estimate of modulated ECCD power[5] for ITER varies from 28 MW for saturated islands to 18 MW for a smaller detectable size of island $w/a \approx 0.04$ (see Figure

[1] O. Sauter, et al., Phys. Plasmas **4** (1997) 1654 M.N. Rosenbluth, Plasma Phys. Control. Fus. **41** (1999)
[2] R.J. La Haye, et al., Phys. Plasmas **7** (2000) 3349
[3] H. Zohm, et al., Proc. 26th EPS Conf. on Controlled Fusion and Plasma Physics (Maastricht, 1999) 1373
[4] G. Giruzzi, et al., Proc. 13th Topical Conf. on Applications of RF Power to Plasmas (Annapolis, USA, April, 1999) A.V. Zvonkov, "Electron Cyclotron Current Drive Optimisation for Control of Neoclassical Tearing Modes in RTO/RC-ITER" unpublished (1999)
[5] V.D. Pustovitov, et al., 18th IAEA Fusion Energy Conference, Sorrento, (2000) IAEA-CN-77/ITERP/07

3.7.4-13), indicating that detection of small islands of $w/a \approx 0.04$ would reduce the required ECCD power to <20 MW.

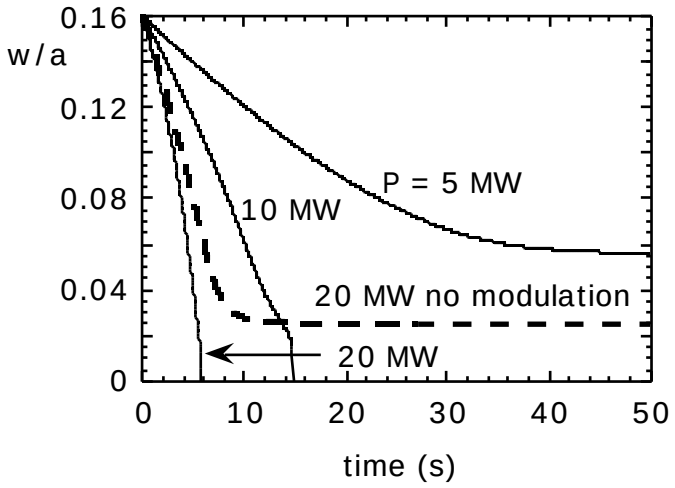

Figure 3.7.4-12 Predictions of Power Requirements and Timescales for (2,1) Neoclassical Tearing Mode Stabilisation by ECCD for Nominal Conditions in a Device with Parameters similar to ITER

Results are shown in terms of the initial island width, w, normalised to the plasma minor radius, a, at ECCD switch-on. It is assumed that the ECCD power is modulated in phase with the island rotation, except for the dashed curve.

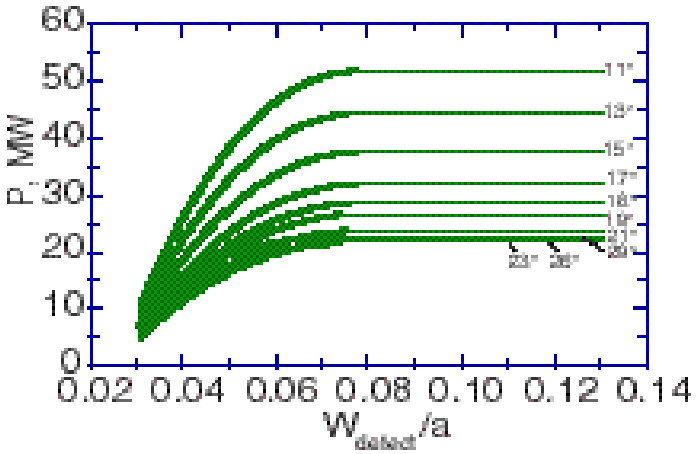

Figure 3.7.4-13 Necessary EC Power (Modulated ECCD) versus Detectable Size of Island for Upper Launching with Angles between the Wavebeam and the Poloidal Plane in a Range $11-29°$ for ITER

The minimum power for the $q=2$ case is obtained for angles between $23°$ and $26°$.

Feedback stabilisation by ECCD seems at present to be the most promising route to ensure control of NTMs in ITER. Direct control of the q profile, shown experimentally to affect the NTM threshold[1], might also be feasible, but requires further investigation. Also, further theoretical work and experimental proof are needed, before it could be recommended to ITER, for the recent proposal[2] to stabilise NTMs by an externally applied static helical field with a helicity different from that of NTMs.

3.7.4.3 Disruption Control

[1] R.J. La Haye, et al., Nucl. Fusion **40** (2000) 53 T.C. Hender, et al., 18th IAEA Fusion Energy Conference, Sorrento, (2000) IAEA-CN-77/EXP3/02
[2] Q. Yu, et al., Phys. Rev. Lett. **85** (2000) 2949

Disruptions and VDEs have a significant effect on the overall design of ITER[1]. The neutral point position in ITER, halo currents, runaway electrons and methods of avoidance and mitigation of the disruptions and VDEs are discussed in this section.

3.7.4.3.1 Plasma Neutral Point Position

Investigation of the vertical instability demonstrates the presence of the so-called passive-stability 'neutral point', where the initial vertical displacement of the plasma magnetic axis or current centroid that occurs after disruption, or fast shutdown β_p loss, is small or zero. The onset of vertical instability following fast shutdown in a vertically-elongated plasma can be avoided if the initial plasma position is chosen to be close to the neutral point. The resulting plasma motion is predominantly radially inward, and a major vertical excursion and the associated halo currents in the upper or lower in-vessel and vessel structures are absent. This type of passive neutral-point instability avoidance was investigated for fast current quenches in JT-60U[2]. The neutral point VDE and halo-current avoidance technique was extended in JT-60U to slow current quenches with active control of the plasma position. Such control is made possible by a plasma-axis vertical position magnetic diagnostic signal that includes compensation for the effect of the toroidal vacuum-vessel eddy currents that develop during the current quench[3]. The resulting actively stabilised single-null divertor plasmas can be controlled vertically down to low plasma current ($\leq$ 10% I_p) and halo currents in the divertor region are avoided. Detailed study of the poloidal field system feasibility of maintaining vertical control after disruption in ITER remains to be performed.

Post-disruption plasma motion was investigated for ITER by means of the DINA code[4]. It has been found[5] that the plasma will generally drift downward for a drop of l_i, upward for a drop of β, and even more significantly upward for any reduction of plasma current. The triangular frames mounted on the vacuum vessel structure to support the lowest blanket modules are an important factor for these motions. The position of the neutral point in ITER is approximately only 10 cm below the plasma centre, thus causing a relatively slow initial plasma speed in response to plasma perturbations.

3.7.4.3.2 Halo Currents

During a vertical disruption (VDE), both the plasma current and cross-sectional area (which encloses toroidal flux) decay to zero. Both decays generate an electric field, which can drive current flow along the helical field lines in the wall-connected scrape-off-layer (SOL) region of the plasma. This so-called 'halo' current[6] flowing helically on wall-intersecting plasma flux surfaces makes a complete circuit by flowing from the strike points at one end of the open SOL field lines, through the conducting first wall structures, and out onto the other end of the

[1] ITER Physics Basis, Chapter 3 Section 4, Nucl. Fusion **39** (1999) 2321
[2] R. Yoshino, Y. Nakamura, Y. Neyatani, Nucl. Fusion **36** (1996) 295
[3] R. Yoshino, J. Koga, T. Takeda, Fusion Technology **30** (1996) 237
[4] R. Khayrutdinov, V. Lukash, J. of Comput. Physics **109** (1993) 193
[5] V. Lukash, Report from ITER Physics Design Group at RRC Kurchatov Institute, "Analysis of RC-ITER Plasma Dynamics during VDE" (2000)
[6] P. NOLL, et al., in Fusion Engineering (Proc. 11th Symposium on Fusion Engineering, Austin 1985), IEEE, New York (1986), **Vol. 1** 33; E.J. Strait, L.L. Lao, J.L. Luxon, E.E. Reis, Nucl. Fusion **31** (1991) 527

SOL field lines. Interaction of the halo current flowing through the wall in the poloidal direction and the toroidal magnetic field produces both vertical and lateral forces. A toroidal asymmetry of the halo current leads not only to local enhancement of the vertical force but also to a net lateral force. The halo current toroidal asymmetry is usually characterised by the toroidal peaking factor TPF, the ratio of maximum halo current density to toroidally averaged halo current density.

The question of the possible tokamak size scaling of the maximum halo current fraction I_h/I_p and TPF is one of the principal remaining uncertainties. Information on the fraction I_h/I_p and TPF in a number of tokamaks assembled as part of the ITER Disruption Database (DDB) indicates that the higher peaking factors tend to be seen only at lower normalized halo currents[1]. The ranges of data from medium-sized and small tokamaks, described in the ITER Physics Basis, are $I_h/I_p \leq 0.4$ (≤ 0.25 typical), $1.2 \leq TPF \leq 4$ and $(I_h/I_p)\times TPF \leq 0.75$ (≤ 0.50 typical)[2]. The database extended with JET and JT-60U data indicates a favourable machine size scaling of $I_{h,max}/I_{p0}$[3], and hence that the bound on maximum halo current fraction in ITER may eventually lie well below ~ 0.3. Furthermore the highest values of TPF x I_h/I_{p0} ~ 0.5 are from low current discharges ($I_p/I_{pmax} = 0.35 - 0.5$, where I_{pmax} is the maximum plasma current achieved in the machine), and the other data satisfy $(I_h/I_p) \times TPF \leq 0.4$. This indicates that the present guideline is conservative.

3.7.4.3.3 Runaway Electrons

The generation of multi-MeV runaway electrons, following onset of plasma disruption at low densities, is a well-known effect in tokamaks. High-current tokamaks such as ITER are theoretically expected to be susceptible to runaway current conversion following disruption even at high density by an avalanche process[4]. The conversion of plasma current magnetic energy to runaway currents leads to localization of the magnetic energy deposition in poloidal direction. Beside this, the first-wall misalignment in the toroidal direction is estimated[5] to increase local deposition by a factor of ~5. Self-consistent studies of ITER runaway conversion and wall-interaction using the DINA code[6] illustrate the potential magnitude of the runaway deposition problem for different post thermal quench values of temperature (T_e = 5 eV, 20 eV, and 35 eV), internal inductance (l_i = 0.7, 0.85 and 1.0) and plasma density ($n_e = 0.6\times10^{20}$ m^{-3}, 0.9×10^{20} m^{-3}, 1.2×10^{20} m^{-3}). Direction of the plasma movement before touching the wall is upwards and to the inner part of the wall. After touching the wall, the plasma moves in the clockwise direction. It is assumed in these calculations that runaway electrons are not confined and that they are expelled from the plasma when the safety factor at the boundary reaches $q_b = 2$, as observed in JT-60U experiments[7]. Because of this effect, the estimated heat load by runaway electron is reduced by an order of magnitude from the

[1] ITER Physics Basis, Chapter 3 Section 4.3.5, Nucl. Fusion **39** (1999) 2343
[2] ITER Physics Basis, Chapter 3 Section 4.3.6, Nucl. Fusion **39** (1999) 2343
[3] R. Yoshino, et al., 17th IAEA FEC (Yokohama,1998) IAEA-CN-69/ITERP1/14
[4] M.N. Rosenbluth, S.V. Putvinski, Nuclear Fusion, **37** (1997) 1355
[5] ITER Physics Basis, Chapter 3 Section 4.4.4, Nucl. Fusion **39** (1999) 2351
[6] V. Lukash, ITER Physics Design Group at RRC "Kurchatov Institute", "Runaway Electrons and Halo Currents in FEAT Plasma", Moscow, (January 2000)
[7] H. Tamai, et al., "Runaway Current Termination in JT60-U", in Proc. of 18th IAEA Fusion Energy Conference, 2000, Sorrento, Italy, IAEA-CN-77-EX9/2

estimate made for ITER-1998 design[1]. The simulations demonstrate that both runaway current I_{ra} and runaway electron energy deposited to the first wall Q_{ra} are diminished with growth of the electron density and/or electron temperature. The runaway current can replace up to the full pre-disruption plasma current, I_{ra} = 14.6 MA at T_e = 5 eV and l_i = 1.0. The maximum Q_{ra} = 25.7 MJ is estimated at T_e = 5 eV and l_i = 0.7.

3.7.4.3.4 Disruption Avoidance and Mitigation of Consequences

ITER components are designed to withstand the electromagnetic and thermal loading stress and erosion consequences of disruptions. The disruption erosion may consume approximately 50% of the overall component lifetime, and sometimes long term reconditioning of plasma-facing surfaces after disruptions will be required before normal plasma operation can be resumed. It is desirable to avoid the occurrence of disruptions whenever possible and to reduce the direct and consequential effects of such disruptions in ITER. The subjects of disruption effect amelioration can be divided into three aspects: (1) *a priori* avoidance of the operation conditions that lead to disruption, (2) active intervention in a discharge scenario after early prediction of disruption onset, and (3) mitigation of unavoidable disruption effects by after-onset actions. All of these methods have been tested and/or demonstrated with some degree of success and reactor relevancy in present tokamaks.

Avoidance of Operation Conditions that Lead to Disruption

The disruptions can, in principle, be avoided during tokamak operation by the use of a discharge scenario which circumvents the various operational limits and conditions that cause disruptions, and by the provision of adequately reliable plasma operation and control systems such that all critical parameters of the prescribed scenario can be reliably obtained and repeated. Operational scenarios to avoid six different types of disruptions were developed in JT-60U[2]. Disruptions caused by the density limit, the error field, β collapse, a high l_i during the plasma current ramp-down at low density, a low l_i during the plasma current ramp-up, and vertical instability, have been studied and successfully avoided in these experiments.

Selection of a scenario that maintains a relatively wide margin against known disruption-initiating conditions is an obvious benefit in the development of such 'disruption-free' scenarios. Under such "reference pulse" conditions, discharges with high plasma performance and low per pulse disruption rates can be obtained. The standard TFTR 'supershot' regimes[3] used for DT experiments were characterised with disruption frequency of ≤ 1%.

Disruption-Onset Predictions

The "reference pulse" scenarios are often based upon conservative plasma operation parameters that do not press close to known disruption-initiating limits or plasma

[1] "Technical Basis for the ITER Final Design Report, Cost Review and Safety Analysis (FDR)", IAEA, Vienna (1998) Chap. III. 62
[2] R. Yoshino, et al., Journal of Japan Society of Plasma Phys. and Contr. Fusion (1994) 1081
[3] E.D. Frederickson, et al., Phys. Plasmas **2** (1995) 4216

configuration control limits. The *a priori* disruption avoidance procedures can in principle be extended to operation scenarios that come closer to several operational limits. In these cases, observation of the limits involved, and provision of real-time disruption prediction (onset warning) capability, become important. Here, monitoring of various plasma performance indicators, including safety factor, internal inductance, plasma density relative to the Greenwald density, radiated power fraction, and status of MHD activity, become essential operation scenario development tools. Monitoring of such indicators can provide warning of the potentially impending onset of disruption. Using a warning indicator to effect feedback-controlled intervention (e.g., feedback[1] from β_N to control P_{add}) can lead to reliable operation near a limit that can initiate disruption.

Basing disruption prediction on single parameter proximity or the confluence of several single parameter limits may not necessarily provide complete certainty for disruption avoidance, or conversely, may unduly restrict the accessible operation domain. A possible improvement can be made by implementation of a neural network disruption predictor, wherein multiple disruption-related indicators or diagnostic signals are combined via a neural network to provide a composite impending disruption warning indicator that is more robust and reliable than simple single- or multiple-parameter indicators. For example, after training, a neural net successfully predicts disruptions in DIII-D[2]. Enhanced predicting capabilities (85%) were achieved in ASDEX Upgrade using a neural network disruption predictor[3]. More complex systems[4] are capable of disruption prediction with a probability of 95%. About 100 disruptions are sufficient to train a neural network. However, how to directly apply training obtained in a present experiment to ITER, or how to shorten the period required for network training in ITER (which will require producing disruptions), remains to be assessed.

The result of any of these prediction methods or of the more traditional approach of detection of disruption MHD precursor growth is an indication of the possible or likely occurrence of a disruption. Such indication can form the basis for initiating avoidance and/or mitigation procedures. The time needed for the implementation of such a procedure determines the 'look-ahead' time-horizon capability needed for the predictor. Reliability of the predictor is a second key consideration: simultaneous achievement of highly reliable prediction of disruption and low (ideally zero) occurrence of 'false alarms' is important.

Softening of the Disruption Consequences

The risk of onset of vertical instability following a disruption in vertically elongated plasma can be reduced if the initial plasma position is chosen to be close to the passive-stability neutral point.

[1] D. Mueller, et al., Fusion Technology **30** (1996) 251
[2] D. Wróblewski, G.L. Jahns, J.A. Leuer, Nucl. Fusion, **37** (1997) 725
[3] G. Pautasso, et al., Journal of Nucl. Materials 290-293 (2001) 1045
[4] F.C. Morabito, et al., "Fuzzi-Neural Approaches to the prediction of disruptions in ASDEX-Upgrade", Nucl. Fusion, to be published; F.C. Morabito, et al., "Progress in the prediction of disruption in ASDEX-Upgrade via neural and fuzzi-neural techniques", in Proc. of 18th IAEA Fusion Energy Conference, 2000, Sorrento, Italy, IAEA-CN-77-EXP3/17

If a full blown VDE can not be avoided, a fast discharge shutdown can be implemented by the injection of impurity or hydrogen species. This injection serves to distribute energy more uniformly by radiation and to limit the severity of VDEs and the resulting vessel vertical and radial forces.

Three methods of injection are being discussed: intense gas puffing, liquid jet injection and solid pellet injection. The pellet injection seems to be most attractive for ITER, although injected impurity may produce runaway electrons. Numerical simulations of the injection of a sequence of 30-50 deuterium pellets doped with a small concentration of krypton with a simultaneous controlled rampdown of the poloidal fieldcoil currents, show that benign fast shutdown without generation of a large number of runaway electrons can be achieved[1]. A cryogenic system for gas pellet preparation is not ideal for stand-by operation. Beryllium pellets or pellets based on polyethylene doped with titanium or silicon are proposed instead of the cryogenic pellets. No long-lived runaway electrons were observed with doped polyethylene pellet injection in ASDEX-Upgrade[2]. Avoidance of runaway electron formation under disruptions was achieved at low values of safety factor, $q_{95} \leq 2$ and in the presence of large-scale magnetic disturbances, $\tilde{B}_r / B_T \approx (2 \div 8) \times 10^{-4}$ in JT-60U[3].

For safety, reduction of fusion power must be achieved in a simple, reliable way. For this purpose, intense impurity gas-puffing will be adequate.

3.7.5 Summary

The ITER Plant Control is achieved by CODAC system, which is structured in a hierarchy composed of the SCS and individual dedicated control subsystems to ensure integrated control of the entire ITER plant.

The SCS supervises the ITER plant operation, controls the plasma discharge, imposes selected plasma parameters, acquires plant and scientific diagnostic data, displays alarms, creates the ITER database, and communicates with both on-site and remote site control rooms.

Control subsystems, dedicated to each plant and diagnostic subsystems, are supervised from a central control system, control directly and monitor the individual plant and diagnostic subsystems, and perform limited actions of autonomous operation of a subsystem even though they are always determined by the supervisory control system.

The above philosophies are adopted to all ITER control systems, and more detailed functional definition and distribution between the SCS and individual subsystems will be determined as for the future work.

The Plasma Control System takes on discharge sequencing, and magnetic, kinetic and disruption control. The poloidal field (PF) system is capable of supporting all the design

[1] Jardin, et al, Nucl. Fusion **40** (2000) 923
[2] Pautasso, et al., Journal of Nucl. Materials 290-293 (2001) 1045
[3] R. Yoshino, S. Tokuda, Nucl. Fusion **40** (2000) 1293

scenarios and the assessed scenario with high plasma current of 17 MA. Simulations show that the PF system can control and recover the plasma position and shape in the case of minor disruptions.

The key elements of kinetic control have been studied for inductive and non-inductive operations. In the inductive operation mode, particle control or helium accumulation determines the time constant of kinetic control, which is typically less than 50 s. Therefore, an inductive burn pulse length of 100-400 s is adequate to investigate transient plasma behaviours. The fusion power can be controlled by fuel density and heating power. The divertor heat load can be controlled by impurity seeding. Stable quasi-steady state plasma will be achieved with various values of Q. High Q operations might be associated with fusion power excursions, which can be suppressed by impurity injection.

For the non-inductive operation mode, time response of plasma parameters to various perturbations (confinement, impurity fraction, current drive power, pumping speed and fuelling rate) has been investigated. Current penetration determines the rate of profile changes and the time constant of any plasma parameter is usually longer than 100 s. A complete current profile relaxation takes about 2000 s, e.g., from a conventional mode to a weak reverse shear mode. However, an almost steady state is achieved within 300 s by optimising the current ramp up phase. Therefore**,** a pulse length longer than 1000 s is not always necessary to study a non-inductive operation mode.

Feedback stabilisation by ECCD system seems to be the most promising route to control neo-classical tearing modes (NTMs). Analyses have shown that detection of small islands ($w/a \sim 0.04$) would enable stabilisation of NTMs by <20 MW of ECCD power.

Reduction of error-field is very important to prevent locked modes. By a Monte-Carlo calculation, the probability is calculated for a range of the error-field amplitude. In non-inductive regimes with $Q > 5$, resistive wall modes (RWMs) pose a major concern since the normalised beta exceeds the ideal limit without the wall. Recent experiments show that reduction of error field is essential to maintain the rotation speed and thus stability at normalised beta above the no-wall limit. A correction coil (CC) system is adequate to reduce the error field and to stabilise these modes. Active stabilisation with this coil system would be necessary in ITER because of difficulty of large momentum input to the plasma to provide sufficient rotation, an alternative stabilising mechanism.

The ITER device is designed to withstand the consequences of disruption (i.e. electromagnetic and heat loads). This assessment is carried out with conservative assumptions based on the experimental database of current quench time and halo current. Experiments show that runaway electrons are eliminated as soon as the boundary safety factor reaches 2, which reduced the estimated heat load by runaway electron by an order of magnitude. A number of disruption prevention and amelioration measures has been tested in recent experiments, e.g. on disruption avoidance by careful selection of discharge scenarios away from the operation limit, prediction of disruption by neural network, and reduction of halo current by strong gas-puff. To summarise, disruption is acceptable for ITER, and the frequency and consequence of disruption can be further reduced in future.